

000
001
002
003
004
005
006
007
008
009
010
011
012
013
014
015
016
017
018
019
020
021
022
023
024
025
026
027
028
029
030
031
032
033
034
035
036
037
038
039
040
041
042
043
044
045
046
047
048
049
050
051
052
053

SOFT QUALITY-DIVERSITY OPTIMIZATION

Anonymous authors

Paper under double-blind review

ABSTRACT

Quality-Diversity (QD) algorithms constitute a branch of optimization that is concerned with discovering a diverse and high-quality set of solutions to an optimization problem. Current QD methods commonly maintain diversity by dividing the behavior space into discrete regions, ensuring that solutions are distributed across different parts of the space. The QD problem is then solved by searching for the best solution in each region. This approach to QD optimization poses challenges in large solution spaces, where storing many solutions is impractical, and in high-dimensional behavior spaces, where discretization becomes ineffective due to the curse of dimensionality. We present an alternative framing of the QD problem, called *Soft QD*, that sidesteps the need for discretizations. We validate this formulation by demonstrating its desirable properties, such as monotonicity, and by relating its limiting behavior to the widely used QD Score metric. Furthermore, we leverage it to derive a novel differentiable QD algorithm, *Soft QD Using Approximated Diversity (SQUAD)*, and demonstrate empirically that it is competitive with current state of the art methods on standard benchmarks while offering better scalability to higher dimensional problems.

1 INTRODUCTION

Optimization in machine learning is typically cast as the search for a single solution that maximizes performance with respect to some objective. Quality-diversity (QD) optimization (Pugh et al., 2016; Chatzilygeroudis et al., 2021) challenges this paradigm by instead discovering a collection of solutions that are both high-performing and behaviorally diverse. This perspective is especially powerful in domains with multiple useful optima, or where robustness and user choice matter as much as raw performance. To illustrate, consider the task of painting a portrait. A traditional optimizer might aim for the single image that is most similar to the subject. Conversely, a QD optimizer not only aims for high fidelity, but also explores a *behavior space* that captures stylistic dimensions like color palette, brushstroke texture, and degree of abstraction, yielding a set of portraits that all resemble the subject while spanning a spectrum of artistic expressions. Such diversity is valuable for human selection and for escaping the limitations of optimizers (Qian et al., 2024) and imperfect objectives.

In recent years, QD optimization has grown from its roots in evolutionary computation into a broadly applicable machine learning paradigm. In reinforcement learning, QD has generated diverse policies that facilitate exploration and improve robustness, in both single (Pierrot et al., 2022; Faldor et al., 2023; Batra et al., 2024) and multi-agent (Ingvarsson et al., 2023) settings. In the context of large foundation models, QD has been adopted for red-teaming and safety analysis (Samvelyan et al., 2024; Wang et al., 2025) as well as diverse content generation (Bradley et al., 2024; Ding et al., 2024). Beyond these, QD has found applications in scenario generation (Bhatt et al., 2022; Fontaine & Nikolaidis, 2022; Zhang et al., 2024), creative design (McCormack & Gambardella, 2022; Zammit et al., 2024), engineering (Sfikas et al., 2023; Hagg et al., 2025), robotics (Huber et al., 2023; Zhong et al., 2023), and scientific discovery (Boige et al., 2023; Janmohamed et al., 2024).

QD algorithms typically operate by partitioning the behavior space into discrete cells and seeking the best solution in each cell (a tessellation, together with the stored solutions, is often referred to as the *archive*). Progress on this objective is commonly measured by the QD Score (Pugh et al., 2016), which sums the performance of the best solutions across all occupied cells, thus capturing both quality and coverage. This approach has fueled much of the progress in QD, including recent advances that incorporate surrogate models (Gaier et al., 2018; Zhang et al., 2022), gradient information (Nilsson & Cully, 2021; Fontaine & Nikolaidis, 2021; 2023), and alternative archive structures

(Vassiliades et al., 2018; Fontaine & Nikolaïdis, 2023; Mouret, 2023). Yet, the formulation also presents two fundamental limitations. First, the non-differentiable nature of tessellations precludes direct optimization using gradient-based optimizers that dominate modern machine learning, except through heuristics (Fontaine & Nikolaïdis, 2021; Nilsson & Cully, 2021). Second, discretizing the behavior space suffers from the curse of dimensionality in high-dimensional setting, as either the number or the volume of cells will grow exponentially, forcing methods to rely on dimensionality reduction techniques such as PCA or autoencoders (Paolo et al., 2020; Grillotti & Cully, 2021; Hedayatian & Nikolaïdis, 2025). As a result, QD optimization remains hindered in high-dimensional, gradient-rich machine learning domains, despite its promise.

We address these challenges by rethinking the formulation of QD optimization itself. We introduce *Soft QD Score* as a new objective for QD optimization that measures how well a collection of solutions cover the behavior space with high-quality solutions, without discretizing the behavior space. Building on it, we derive *SQUAD*, a novel algorithm that leverages a tractable lower bound of the Soft QD score to enable end-to-end differentiable optimization. This approach has an intuitive interpretation as finding an equilibrium between attractive forces, which drive solutions toward higher quality, and repulsive forces, which spread them across the behavior space. Through experiments on both established and newly designed QD benchmarks, we demonstrate that SQUAD broadens the applicability of QD and provide further insights into its properties.

Our contributions are threefold: 1. We introduce Soft QD, a new formulation of QD optimization and analyze its theoretical properties. 2. We develop SQUAD, a differentiable QD algorithm derived from the aforementioned formulation. 3. We evaluate SQUAD on multiple benchmarks, showing its effectiveness in high-dimensional and complex optimization settings.

2 BACKGROUND

The quality diversity (QD) problem aims to find a collection of high-quality solutions that are diverse in their behavior. A QD problem is defined by a solution space Θ , an *objective or quality function* $f : \Theta \rightarrow \mathbb{R}$ which measures a solution's quality, and a *behavior descriptor function* $\text{desc} : \Theta \rightarrow \mathcal{B}$ that maps each solution to a point in the *behavior space* \mathcal{B} . The goal is to discover for each point in \mathcal{B} a high-quality solution that exhibits that specific behavior. We can formalize this objective as finding a set of solutions $\boldsymbol{\theta} = \{\theta_b\}_{b \in \mathcal{B}}$ that maximizes the integral of their quality over the behavior space, $\int_{\mathcal{B}} f(\theta_b) \, d\theta$. The problem is referred to as Differentiable Quality-Diversity (DQD) (Fontaine & Nikolaïdis, 2021) when both the objective and descriptor functions are differentiable.

Since the behavior space \mathcal{B} is continuous, QD algorithms often partition it into n cells, $\mathcal{A} = \{c_1, \dots, c_n\}$, known as an *archive* or *tessellation*. The QD objective is then framed as finding a high-quality solution for each cell. This is captured by the *QD Score*, which is the sum of the maximum quality found within each cell:

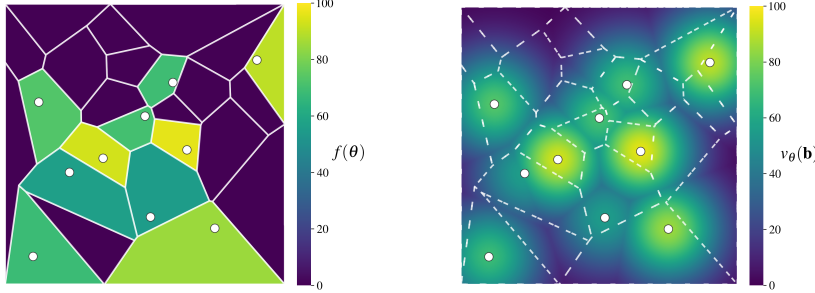
$$\max_{\boldsymbol{\theta}} \text{QD Score}_{\mathcal{A}}(\boldsymbol{\theta}) = \sum_{c \in \mathcal{A}} \max\{f(\theta) : \theta \in \boldsymbol{\theta}, \text{desc}(\theta) \in c\}. \quad (1)$$

Discretizing the behavior space introduces a fundamental challenge in high dimensions due to the curse of dimensionality. Grid archives (e.g., Cully et al. (2015)) divide the space evenly along each dimension, which makes the number of cells grow exponentially with the dimensionality of \mathcal{B} . This makes it infeasible to maintain a fine-grained grid when \mathcal{B} is high-dimensional. Centroidal Voronoi Tessellation (CVT) archives (Vassiliades et al., 2018) address this by fixing the number of cells and defining them around a set of centroids. Each cell contains all points that are closer to its assigned centroid than to any other centroid, creating an almost uniform partitioning of the space. While this avoids the exponential increase of the number of cells, the volume of each CVT cell still grows exponentially with dimensionality. Large cells make it difficult to explore new regions by building on existing solutions (which is commonly done in QD methods), since reaching a different cell would likely require substantial changes to a current solution. Consequently, both discretization strategies face practical limitations in high-dimensional behavior spaces, either requiring an infeasibly large number of cells or forcing exploration across cells that are too large to navigate effectively.

108

3 SOFT QUALITY-DIVERSITY

109

110 To overcome the challenges of discretizing the behavior space, we introduce *Soft QD Score*, an
111 objective for quality-diversity that forgoes tessellations. Conceptually, our approach builds on the
112 view of QD algorithms as a form of “illumination” (Cully et al., 2015). We treat each solution as
113 a light source that illuminates the behavior space, where its brightness is proportional to its quality.
114 A set of solutions is then evaluated based on how well they illuminate the entire behavior space.
115 This contrasts with traditional approaches, where a discrete cell is considered fully illuminated by
116 its single best occupant. In Soft QD, solutions contribute to illuminating multiple regions, with their
117 influence decaying smoothly as a function of distance. Figure 1 illustrates this difference.

128 Figure 1: **Left:** In a discrete archive, each cell is fully illuminated by its highest-quality occupant.
129 **Right:** In Soft QD, each solution illuminates the area around with an intensity proportional to its
130 quality. The smooth scalar field defined by the behavior value $v_\theta(\mathbf{b})$ is independent of discretization.
131 Formally, to assess a population of solutions $\theta = \{\theta_1, \dots, \theta_N\}$, we first define the **behavior value**
132 $v_\theta(\mathbf{b})$ that it induces at any point \mathbf{b} in the behavior space as

133
$$v_\theta(\mathbf{b}) = \max_{1 \leq n \leq N} f_n \exp\left(-\frac{\|\mathbf{b} - \mathbf{b}_n\|^2}{2\sigma^2}\right), \quad (2)$$
134
135

136 where $f_n = f(\theta_n)$ and $\mathbf{b}_n = \text{desc}(\theta_n)$ are the quality and behavior descriptors of solution θ_n ,
137 respectively, and σ is a kernel width parameter. We use the Gaussian kernel, in line with its standard
138 application in methods like density estimation (Bishop, 2007), to model a smooth, localized field of
139 influence for each solution. Intuitively, $v_\theta(\mathbf{b})$ measures the quality of the best available solution for
140 a target behavior \mathbf{b} , discounted exponentially by its distance in behavior space. If the population
141 contains a solution whose behavior \mathbf{b}_n perfectly matches \mathbf{b} , the behavior value $v_\theta(\mathbf{b})$ will be at
142 least as large as its quality f_n . Conversely, $v_\theta(\mathbf{b})$ approaches zero when there are no high-quality
143 solutions near \mathbf{b} . Figure 2 illustrates how the scalar field of behavior values changes as the solutions
144 move around in the behavior space.

145 The total behavior value that a population θ induces over the entire behavior space measures its
146 combined quality and diversity. We call this quantity **Soft QD Score** and formally define it as:

147
$$S(\theta) = \int_{\mathcal{B}} v_\theta(\mathbf{b}) d\mathbf{b}. \quad (3)$$
148
149

150 The term “Soft” highlights a key difference from the traditional QD Score. Instead of a hard assign-
151 ment of solutions to discrete cells, here each solution continuously contributes to the illumination
152 of the behavior space. Soft QD Score captures our expectations of a QD solution. To obtain a high
153 value, the population must contain high-quality solutions spread across the behavior space. More-
154 over, adding new solutions to a population will only ever increase the value of the population, and so
155 does increasing the quality of existing solutions. The following theorem, formally stated and proven
156 in Appendix B, establishes some of these properties. Furthermore, this theorem provides additional
157 grounding for Soft QD Score by connecting its limiting behavior to the conventional QD Score.

158 **Theorem 1** (Informally stated). *The Soft QD Score, as defined in Eq. 3, satisfies the following
159 properties:*

160 **Monotonicity.** *The value is non-decreasing with respect to the addition of new solutions and the
161 improvement of existing solution qualities.*

162 **Submodularity.** *The value is a submodular set function.*

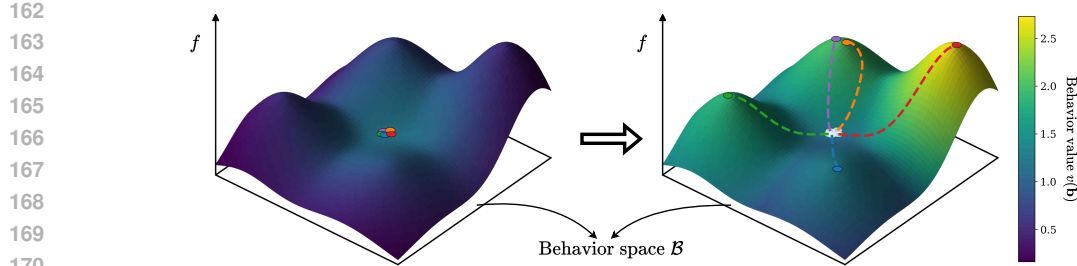


Figure 2: **Optimizing Soft QD Score with SQUAD.** The plots visualize the behavior value function, $v_\theta(\mathbf{b})$, induced by a population of five solutions. The bottom plane represents the behavior space \mathcal{B} , the height corresponding to solution quality, f , and the colored surface shows the induced behavior value v_θ . Initially (left), a cluster of low-quality solutions induces a low behavior value. As SQUAD improves the population (right), the induced behavior value increases in both magnitude and coverage, leading to a higher Soft QD Score.

Limiting Equivalence. *In the limit as $\sigma \rightarrow 0$, the Soft QD Score converges (up to a constant factor) to the traditional QD score on a fine-grained archive.*

4 SQUAD: SOFT QD USING APPROXIMATED DIVERSITY

Directly maximizing the Soft QD Score of a population, $S(\theta)$, is challenging as it involves an integral over the behavior space. We can, however, maximize a tractable lower bound. Theorem 2 establishes such a bound, which forms the basis of our algorithm.

Theorem 2. *Given a population $\theta = \{\theta_n\}_{n=1}^N$ with qualities $\{f_n\}_{n=1}^N$ and behavior descriptor vectors $\{\mathbf{b}_n\}_{n=1}^N$ in behavior space $\mathcal{B} = \mathbb{R}^d$, its Soft QD Score $S(\theta)$ can be approximated by a lower bound $\tilde{S}(\theta)$ defined as:*

$$\tilde{S}(\theta) = (2\pi\sigma^2)^{\frac{d}{2}} \left[\sum_{n=1}^N f_n - \sum_{1 \leq i < j \leq N} \sqrt{f_i f_j} \exp\left(-\frac{\|\mathbf{b}_i - \mathbf{b}_j\|^2}{8\sigma^2}\right) \right] \quad (4)$$

A proof is provided in Appendix A.1.

Our algorithm, **Soft QD Using Approximated Diversity** (SQUAD), iteratively improves a randomly initialized population of N solutions by updating its constituent solutions to maximize this lower bound. For brevity, we drop the leading constant $(2\pi\sigma^2)^{\frac{d}{2}}$ as it does not affect the optima. Furthermore, we rename $8\sigma^2$ as γ^2 which, as we shall see in Section 5.3, controls the quality-diversity trade-off. Therefore, with some slight abuse of notation, we define the SQUAD objective $\tilde{S}(\theta)$ as:

$$\tilde{S}(\theta) = \sum_{n=1}^N f_n - \sum_{1 \leq i < j \leq N} \sqrt{f_i f_j} \exp\left(-\frac{\|\mathbf{b}_i - \mathbf{b}_j\|^2}{\gamma^2}\right) \quad (5)$$

Assuming that the quality and behavior descriptor functions (f and desc) are differentiable, this objective will also be fully differentiable with respect to the solutions' parameters. Hence, we can use a modern optimizer like Adam (Kingma & Ba, 2015) to iteratively update a population to improve its combined quality and diversity. This objective also has a remarkably simple interpretation. Essentially, it is composed of two summation terms:

- A **quality term** $\sum f_n$ which encourages all solutions to have higher qualities.
- A **diversity term** that acts as a pairwise repulsion, penalizing solutions that are behaviorally close.

The diversity term penalizes behavioral similarity through a sum over solution pairs. Each pair's penalty is the product of two components: the geometric mean of their qualities, $\sqrt{f_i f_j}$, and an exponential term that increases with their proximity. The combination of these two terms heavily penalizes high-quality solutions that are behaviorally similar. Notably, the geometric mean term

216 **Algorithm 1** Soft QD Using Approximated Diversity (SQUAD)

217 **Require:** Optimizer O , learning rate η , population size N , batch size M , neighbors K , epochs
218 T_{\max} , kernel bandwidth γ^2 .

219 **Require:** Differentiable evaluation function $\text{Eval}(\theta)$ returning quality f and descriptor \mathbf{b} .

220 1: **Initialize:**

221 2: Population $\boldsymbol{\theta} = \{\theta_i\}_{i=1}^N$

222 3: Evaluations $(F, B) \leftarrow \text{Eval}(\boldsymbol{\theta})$

223 4: Optimizer state $\mathcal{S} \leftarrow O.\text{init}(\boldsymbol{\theta})$

224 5: **for** $t = 1$ to T_{\max} **do**

225 6: **for** each batch of indices $\mathcal{I} \subseteq \{1, \dots, N\}$ **do**

226 7: For each $i \in \mathcal{I}$, find neighbor indices $\mathcal{N}_i \leftarrow K\text{-Nearest-Neighbors}(\mathbf{b}_i, B)$

227 8: Compute objective function for batch:

228 9: $\tilde{S}_{\mathcal{I}}(\boldsymbol{\theta}) \triangleq \sum_{i \in \mathcal{I}} f_i - \frac{1}{2} \sum_{i \in \mathcal{I}, j \in \mathcal{N}_i} \sqrt{f_i f_j} \exp\left(-\frac{\|\mathbf{b}_i - \mathbf{b}_j\|^2}{\gamma^2}\right)$

229 10: Update parameters: $(\boldsymbol{\theta}_{\mathcal{I}}, \mathcal{S}_{\mathcal{I}}) \leftarrow O.\text{update}(\boldsymbol{\theta}_{\mathcal{I}}, G_{\mathcal{I}}, \mathcal{S}_{\mathcal{I}}, \eta)$

230 11: Update evaluations for the batch: $(F_{\mathcal{I}}, B_{\mathcal{I}}) \leftarrow \text{Eval}(\boldsymbol{\theta}_{\mathcal{I}})$

231 12: **end for**

232 13: **end for**

233 14: **return** Final population $\boldsymbol{\theta}$

235

236

237

238 discounts the similarity penalty for low-quality solutions, allowing them to first prioritize quality
239 optimization before gradually shifting to optimize for behavioral diversity as qualities increase.

240 The presence of pairwise interactions in the diversity term is a direct consequence of the second-
241 order approximation we used to derive the bound in Theorem 2. Although higher-order interactions
242 between triplets and larger groups of solutions also exist in the full integral, our approximation
243 considers only the most significant pairwise terms. As our analysis in Appendix A.2 shows, the
244 component of approximation error originating from ignoring the higher-order interactions decreases
245 as the solutions spread out. Therefore, as the solutions spread out during optimization, ignoring
246 higher-order interactions becomes less detrimental to the accuracy of the approximation.

247 Building on this objective, we next describe two additional components needed for an efficient
248 algorithm.

249

250 **Efficient computation with batches and nearest neighbors.** A naive implementation of the
251 SQUAD objective in Eq. 5 requires computing and applying $\mathcal{O}(N^2)$ pairwise repulsions, which
252 is computationally prohibitive for large populations. To overcome this, we only compute the repul-
253 sion for each solution from its k -nearest neighbors in the behavior space. This reduces the number
254 of gradient updates that needs to be calculated at each iteration to $\mathcal{O}(Nk)$. The omission of far-
255 ther solutions from the calculation is justified by the exponential decay of the repulsive force with
256 distance, which quickly makes the contribution from distant solutions negligible. Additionally, to
257 manage the memory and computational cost per gradient step, we update the population in mini-
258 batches rather than all at once. In Appendix C.2 and C.1 we report the results of ablation studies on
259 the choice of k and the batch size, which show the robustness of SQUAD to these hyperparameters.

260

261 **Handling bounded behavior spaces.** Our derivation of the SQUAD objective assumes an un-
262 bounded behavior space $\mathcal{B} = \mathbb{R}^d$. However, many problems, including our experiments, have in-
263 trinsically bounded behavior descriptors. While extending the derivation to bounded domains is
264 possible, it leads to a significantly more complex and potentially less stable final objective. We
265 instead adopt a simpler approach: we transform the bounded space into an unbounded one using
266 the logit function. Specifically, we map each point in the bounded behavior space $\mathbf{b} \in [0, 1]^d$ to
267 $\mathbf{b}' = \log \frac{\mathbf{b}}{1-\mathbf{b}} \in \mathbb{R}^d$. We found this choice to be critical for the success of the algorithm, and ablated
268 it in Appendix C.3 to confirm its importance.

269 Putting these pieces together, Algorithm 1 presents a complete pseudocode for SQUAD.

270

5 EXPERIMENTS

271
 272 Our experiments are designed to comprehensively evaluate SQuAD and answer three key questions.
 273 First, how does SQuAD scale with the dimensionality of the behavior space? Second, how does it
 274 navigate the fundamental trade-off between solution quality and population diversity? Lastly, how
 275 does SQuAD compare with state-of-the-art methods on complex, high-dimensional optimization
 276 problems? To answer these questions, we evaluate SQuAD and several baselines on three bench-
 277 mark domains, each selected to probe one of these specific aspects.
 278

279

5.1 EXPERIMENTAL SETUP

280 **Benchmark domains** We evaluate different facets of QD optimization on three benchmarks, de-
 281 scribed below and in detail in Appendix D.1.

282 **Linear Projection (LP):** Following Fontaine et al. (2020), an algorithm must maximize an objective
 283 while maintaining diversity in a d -dimensional behavior space defined by a linear projection of the
 284 solution vector. We use the multi-modal Rastrigin function (Rastrigin, 1974), making this a simple
 285 yet challenging testbed for analyzing scalability with respect to d .

286 **Image Composition (IC):** Inspired by computational creativity tasks (Tian & Ha, 2022; Ibarrola
 287 & Grace, 2023), this benchmark adjusts the parameters of a set of circles (position, radius, color,
 288 transparency) to reconstruct a target image. A solution’s quality is its similarity to the target image,
 289 while a 5-d behavior space encodes properties such as color harmony. The moderately sized behav-
 290 ior space and challenging optimization make it ideal for analyzing the quality-diversity trade-off.

291 **Latent Space Illumination (LSI):** Based on Fontaine & Nikolaidis (2021), algorithms search the
 292 latent space of StyleGAN2 (Karras et al., 2020) to generate images matching a target text prompt.
 293 Following Fontaine & Nikolaidis (2023), we target images of “Tom Cruise” while diversifying in
 294 age and hair length. We also propose a harder version with a 7-d behavior space in which we target
 295 images of “a detective from a noir film”. Both objective and behavior descriptors use CLIP (Radford
 296 et al., 2021) embeddings to evaluate the similarity between generated images and given texts. This
 297 serves as our most difficult domain for testing QD algorithms.
 298

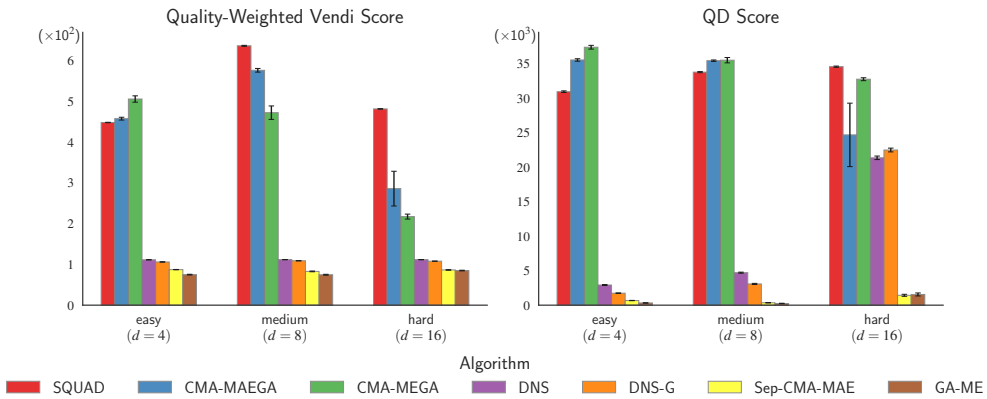
299 **Baselines** We compare SQuAD against state-of-the-art algorithms for high-dimensional and dif-
 300 ferentiable QD, using the open source pyribs (Tjanaka et al., 2023b) implementations: CMA-
 301 MAEGA (Fontaine & Nikolaidis, 2023), CMA-MEGA (Fontaine & Nikolaidis, 2021), and Sep-
 302 CMA-MAE (Tjanaka et al., 2023a). We also include Gradient-Assisted MAP-Elites (GA-ME),
 303 which adapts the policy-gradient-based algorithm PGA-ME Nilsson & Cully (2021) to the DQD
 304 setting by using direct gradients from the objective function (GA-ME is also similar to the OG-
 305 MAP-Elites (line) baseline in Fontaine & Nikolaidis (2021)). To ensure a fair comparison in high-
 306 dimensional behavior spaces, all baselines use Centroidal Voronoi Tesselation (CVT) to discretize
 307 the behavior space into a fixed-size archive Vassiliades et al. (2018). In addition to these methods, we
 308 also include DNS (Bahlous-Boldi et al., 2025) which is a modern variant of novelty search (Lehman
 309 & Stanley, 2011) used for QD optimization in more complex domains. We also include an improved
 310 variant of it that uses gradient-based updates (similar to GA-ME) to complement its regular muta-
 311 tion operator. We denote this variant as DNS-G. Additional details about the hyperparameters of the
 312 algorithms are presented in Appendix D.3.

313
 314 **Evaluation metrics** To provide a thorough analysis of the trade-offs offered by each algorithm,
 315 we use several metrics to measure the quality and diversity of the generated populations.
 316 For quantifying diversity, we primarily use the *Vendi Score (VS)* (Friedman & Dieng, 2023), which
 317 quantifies the effective number of distinct clusters in a population. We supplement this with *Cover-
 318 age* which is the percentage of occupied cells in a fixed CVT archive. To understand the quality of
 319 the generated populations, we report the *Maximum Quality* to assess pure optimization performance
 320 and the *Mean Quality* to evaluate the overall quality of solutions across the entire population. Fi-
 321 nally, to compare the overall performances, we use *QD Score* (Pugh et al., 2016) which measures
 322 the sum of qualities in a fixed CVT archive and *Quality-weighted Vendi Score (QVS)* (Nguyen &
 323 Dieng, 2024) which extends Vendi Score to account for the quality of a population as well. A full
 324 definition of all of the metrics and further discussion is provided in Appendix D.2.

324 5.2 SCALABILITY TO HIGH-DIMENSIONAL BEHAVIOR SPACES
325

326 To evaluate SQUAD’s scalability to high-dimensional behavior spaces, we conducted three sets of
327 experiments on the LP benchmark, using 4, 8, and 16-dimensional behavior spaces. As shown in
328 Figure 3, methods that leverage gradient information from descriptors (SQUAD, CMA-M(A)EGA)
329 perform much better than methods that do not (Sep-CMA-MAE, GA-ME, DNS) which highlights
330 the difficulty of exploring high-dimensional behavior spaces without gradients. To assess statistical
331 significance of the results in Figure 3, we evaluated algorithm performance per task and metric using
332 Kruskal-Wallis tests (all $p < 0.001$) followed by Holm-Bonferroni-corrected Mann-Whitney U tests
333 to compare the best algorithm against the others. All differences were significant ($p < 0.001$) except
334 for CMA-MAEGA on medium ($d = 8$) and hard ($d = 16$) tasks for QD Scores, where it was not
335 significantly different from the top-performing algorithms; in the hard domain, this is primarily due
336 to the high variance of CMA-MAEGA.

337 While CMA-MEGA and CMA-MAEGA have a slight edge in the 4-dimensional behavior space,
338 SQUAD closes this gap and noticeably outperforms them in the more challenging versions of the
339 task. We attribute the initial success of CMA-M(A)EGA to their large archives (10^4 cells), which
340 are dense enough to effectively cover the low-dimensional space. However, as the dimensionality
341 increases, the density of their archives drops exponentially, making the feedback less informative.
342 This limitation is a key reason for their performance decline in higher-dimensional spaces. SQUAD,
343 on the other hand, does not discretize the behavior space which enables it to maintain strong per-
344 formance as dimensionality increases. Furthermore, SQUAD demonstrates greater stability across
345 all three tasks, with the lowest variance across different evaluations. More detailed results of these
346 experiments are presented in Appendix E.



360 **Figure 3: QVS (left) and QD Score (right) on LP tasks with increasing behavior descriptor**
361 **dimensionality** (4, 8, 16). All results are averaged over 10 runs, with error bars depicting the
362 standard errors. SQUAD’s performance relative to the baselines improves with task complexity,
363 with it outperforming all other methods on the most challenging 16-d task for both metrics.

364 5.3 ANALYSIS OF THE QUALITY-DIVERSITY TRADE-OFFS
365

366 Obtaining diversity often comes at the expense of quality. In this section, we shed some light on
367 the quality-diversity tradeoff that SQUAD offers in comparison to baseline algorithms using the IC
368 domain, which provides a realistic optimization challenge with a moderately sized, 5-d behavior
369 space. We also examined the bandwidth parameter, γ^2 , and showed that it acts as a knob, allowing
370 SQUAD to effectively trade off quality for diversity.

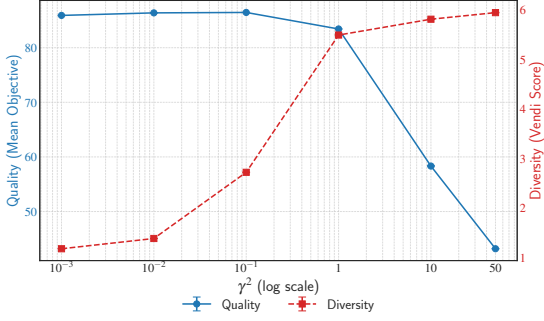
371 As the results in Table 1 indicate, SQUAD outperforms the baselines on most metrics. The average
372 quality of the solutions found by SQUAD is significantly higher than those of the baselines. Further-
373 more, the high quality of the best solution in SQUAD’s population shows that it is highly capable
374 in pure quality optimization. On diversity metrics, SQUAD maintains its noticeable lead on Vendi
375 Score but falls short of CMA-MAEGA on Coverage by a small margin. The discrepancy between
376 the two diversity metrics can be explained by the fact that Vendi Score takes the shape of the archive
377 into account. Therefore, while the larger number of solutions found by CMA-MAEGA helps it

378
 379
 380
 381
Table 1: Performance in the IC domain. Comparing SQuAD ($\gamma^2 = 1$) with baselines in terms
 382 of the quality (Best Objective, Mean Objective) and diversity (Vendi Score, Coverage). Results are
 383 mean \pm standard error averaged over 10 runs, with the best score for each metric shown in **bold**.
 384
 385

| Algorithm | Quality | | Diversity | |
|-------------|------------------------------------|------------------------------------|-----------------------------------|-----------------------------------|
| | Mean Objective | Max Objective | Vendi Score | Coverage |
| SQuAD | 83.37 \pm 0.02 | 93.58 \pm 0.10 | 5.49 \pm 0.00 | 5.68 \pm 0.06 |
| CMA-MAEGA | 74.83 \pm 0.20 | 88.79 \pm 0.92 | 3.93 \pm 0.03 | 5.85 \pm 0.05 |
| CMA-MEGA | 75.98 \pm 0.26 | 86.18 \pm 1.58 | 3.25 \pm 0.24 | 4.54 \pm 0.49 |
| DNS | 71.30 \pm 0.15 | 74.54 \pm 0.18 | 1.62 \pm 0.01 | 1.52 \pm 0.02 |
| DNS-G | 74.49 \pm 0.03 | 76.48 \pm 0.11 | 1.67 \pm 0.00 | 1.49 \pm 0.03 |
| Sep-CMA-MAE | 72.15 \pm 0.21 | 74.57 \pm 0.04 | 1.32 \pm 0.01 | 0.46 \pm 0.02 |
| GA-ME | 73.44 \pm 0.41 | 74.53 \pm 0.45 | 1.14 \pm 0.04 | 0.19 \pm 0.03 |

392
 393 cover the behavior space more densely, this coverage is concentrated in a smaller region, leading to
 394 its lower Vendi Score. This is further supported by the archive visualizations in Appendix E.
 395

396 Having compared SQuAD with the base-
 397 lines, we examined how to control its quality-
 398 diversity tradeoff via the bandwidth parame-
 399 ter, γ^2 . As Equation 5 suggests, increasing γ^2
 400 boosts the contribution of the diversity term
 401 by increasing its effective range and intensity.
 402 Empirically, we confirmed this by evaluating
 403 SQuAD with different values of γ^2 ranging
 404 from 10^{-3} to 50 in the IC domain. As Figure 4
 405 shows, increasing γ^2 indeed improves the di-
 406 versity of the solutions, albeit at the price of
 407 their quality. These results show how SQuAD
 408 lets the users trade off quality for diversity
 409 (and vice versa) by changing the value of a
 410 single hyperparameter.



411
 412
**Figure 4: Controlling the quality-diversity trade-
 413 off with γ^2 .** The plot shows how varying γ^2 im-
 414 pacts solution quality, measured by the mean ob-
 415 jective (blue line), and diversity, measured by the Vendi
 416 Score (dashed red line).
 417

5.4 PERFORMANCE ON CHALLENGING DQD PROBLEMS

418 In our last set of experiments, we compared SQuAD with baselines on the challenging LSI domain.
 419 In line with prior work (Fontaine & Nikolaidis, 2023) we searched the latent space of StyleGAN2 for
 420 latents that would generate images of Tom Cruise and are diverse with respect to age and hair length.
 421 Additionally, we also set up a more challenging version of the LSI benchmark with a 7-d behavior
 422 space. In this more difficult task the goal is to generate “photos of a detective from a noir film” and
 423 the images have to be diverse with respect to different attributes including facial expression, pose,
 424 and hair color. Additional details about both versions of LSI is presented in Appendix D.1.3.

425
 426 **Table 2: Performance in the Latent Space Illumination (LSI) domain.** Results are averaged over
 427 5 runs and reported as mean \pm standard error, with the best scores highlighted in **bold**. Algorithms
 428 that failed to achieve a positive mean objective (hence, have a zero QVS) are shown with *.
 429

| Algorithm | LSI | | LSI (Hard) | |
|-------------|------------------------------------|-----------------------------------|-----------------------------------|-----------------------------------|
| | QD Score ($\times 10^3$) | QVS | QD Score ($\times 10^3$) | QVS |
| SQuAD | 13.41 \pm 0.19 | 177.0 \pm 2.8 | 2.55 \pm 0.08 | 151.3 \pm 0.1 |
| CMA-MAEGA | 6.82 \pm 0.10 | 121.6 \pm 9.7 | 0.39 \pm 0.07 | 99.3 \pm 1.0 |
| CMA-MEGA | 8.70 \pm 0.07 | 140.1 \pm 1.7 | 0.27 \pm 0.05 | 92.8 \pm 1.5 |
| DNS | -9.31 \pm 2.52 | 0.0 \pm 0.0* | -11.27 \pm 1.46 | 0.0 \pm 0.0* |
| DNS-G | -8.53 \pm 1.50 | 0.0 \pm 0.0* | -6.81 \pm 0.47 | 0.0 \pm 0.0* |
| Sep-CMA-MAE | -0.59 \pm 0.45 | 0.0 \pm 0.0* | 0.02 \pm 0.04 | 0.0 \pm 0.0* |
| GA-ME | -14.90 \pm 1.67 | 0.0 \pm 0.0* | 0.08 \pm 0.00 | 0.0 \pm 0.0* |

The performance of different algorithms are compared in terms of QD Score and Quality-weighted Vendi Score in Table 2. In both LSI tasks, SQUAD outperforms the baselines by a significant margin, showcasing its capability in challenging domains. A closer inspection of the data (available in Appendix E) reveals that SQUAD is particularly adept in exploring the behavior space. Thus, despite performing similar to the baselines in terms of mean quality, SQUAD’s ability to maintain a better coverage of the behavior space differentiates it from the baselines. Similar to our prior results, Sep-CMA-MAE and GA-ME perform poorly on both versions of the LSI task. Here, we attribute their poor performance to the high-dimensional and non-linear nature of the optimization landscape, which makes it difficult to navigate the behavior space. Interestingly, GA-ME, despite using gradient ascent updates, is unable to effectively escape local optima, highlighting the important role of modern optimizers in more challenging domains.

6 RELATED WORK

Quality-diversity (QD) optimization has recently become a topic of interest in machine learning, following the introduction of the NSLC (Lehman & Stanley, 2011) and MAP-Elites (Cully et al., 2015) algorithms. MAP-Elites, as a canonical QD algorithm, uses random mutations to find solutions that occupy different behavioral *niches* in a tessellated behavior space. This general recipe is improved by methods that have proposed better discretization schemes (Vassiliades et al., 2018; Mouret, 2023), incorporated modern evolutionary optimizers (Fontaine et al., 2020; Tjanaka et al., 2023a; Batra et al., 2024; Choi & Togelius, 2021), and improved the search by using gradient-aware mutations (Nilsson & Cully, 2021; Pierrot et al., 2022; Faldor et al., 2023) and crossovers (Ingvarsson et al., 2023). It is worth noting that these advancements rely on discrete archives, which are known to be sensitive to the archive resolution (Fontaine & Nikolaidis, 2023). To the best of our knowledge, the only other work that proposes a discretization-free formulation of QD is the continuous QD Score of Kent et al. (2022). Continuous QD Score is similar to SoftQD Score in that both compute an integral over the behavior space. However, continuous QD Score employs a non-smooth kernel, which makes it difficult to approximate analytically and restricts estimation to Monte Carlo sampling methods. Consequently, it is used exclusively as an evaluation metric rather than as an optimization objective. Another major contribution was the formulation of differentiable QD (Fontaine & Nikolaidis, 2021) where the quality and behavior descriptor functions are assumed to be differentiable. This, along with the introduction of gradient arborescence algorithms (Fontaine & Nikolaidis, 2023) paved the way for QD algorithms to tackle large scale optimization problems (Yu et al., 2025; Wan et al., 2025). Our work is a continuation of this trend that frames the whole QD problem as a unified optimization problem, enabling seamless integration with modern gradient-based optimizers.

The pairwise repulsive term in SQUAD’s objective is reminiscent of the kernel-based repulsion used in particle variational inference methods such as Stein Variational Gradient Descent (SVGD) (Liu & Wang, 2016), where particles are simultaneously attracted toward regions of high target density and repelled from one another to prevent collapse. Unlike QD, these methods aim to approximate a probability distribution rather than optimize quality while diversifying in a behavior space, which does not exist in SVGD or its reinforcement learning variant, SVPG (Liu et al., 2017). Nonetheless, recent SVGD advances for high-dimensional inference, including message passing (Zhuo et al., 2018), matrix-valued kernels (Wang et al., 2019), and Newton-like updates (Chen et al., 2019), offer practical ideas for stabilizing and scaling repulsive forces that could be adapted to SQUAD’s objective. Lastly, a related example outside variational inference is DOMiNO (Zahavy et al., 2023), which enforces diversity in reinforcement learning via repulsive forces and a Lagrangian formulation, showing the broader utility of such mechanisms for balancing quality with diversity.

7 CONCLUSION

In this work, we introduced Soft QD as a new formulation of QD optimization that does not require discretizing the behavior space. Building on it, we proposed SQUAD, a novel QD algorithm tailored for differentiable domains. Our experiments across multiple benchmarks demonstrated that SQUAD achieves competitive performance with state-of-the-art methods, and exhibits promising scalability to higher-dimensional behavior spaces. In addition, we highlighted how it enables a convenient trade-off between quality and diversity, offering a fresh perspective on the design of QD algorithms.

486 Despite the encouraging results, several limitations remain. First, the current formulation of SQUAD
 487 assumes differentiable objectives and behavior descriptors, which may be costly to obtain or unavail-
 488 able in certain domains. Extending Soft QD to reinforcement learning settings with estimated
 489 gradients, or to fully non-differentiable domains via evolutionary strategies, represents a promising
 490 direction, where issues such as navigating deceptive behavior landscapes may pose unique challenges.
 491 Second, our analysis in Section 5.3 showed the critical role of the kernel bandwidth, γ in shaping
 492 the quality-diversity trade-off of SQUAD. Future work could investigate adaptive or per-solution
 493 schedules for γ , for example by adjusting it based on the distribution of solutions or by annealing it
 494 during training. Moreover, while SQUAD’s second-order approximation of the Soft QD Score of-
 495 fers tractability, it also discards higher-order interactions. Alternatives such as sparsification of the
 496 interactions, message-passing, or Monte Carlo approaches may provide richer modeling of interac-
 497 tions, though potentially at higher computational cost. Lastly, while we use a logit transformation
 498 to handle bounded behavior spaces, exploring alternative transformations could be an avenue for
 499 future work to further improve performance. Taken together, we introduce Soft QD as a powerful
 500 conceptual tool and SQUAD as a practical algorithm, highlighting a new path for quality-diversity
 501 in complex, differentiable domains. We hope this work inspires the community to build upon this
 502 foundation, realizing the full promise of scalable and general purpose QD.

503 REFERENCES

504

505 Ryan Bahlous-Boldi, Maxence Faldor, Luca Grillotti, Hannah Jammohamed, Lisa Coiffard, Lee
 506 Spector, and Antoine Cully. Dominated novelty search: Rethinking local competition in quality-
 507 diversity. In *Proceedings of the Genetic and Evolutionary Computation Conference, GECCO
 508 2025, NH Malaga Hotel, Malaga, Spain, July 14-18, 2025*, pp. 104–112. ACM, 2025. URL
 509 <https://doi.org/10.1145/3712256.3726310>.

510 Sumeet Batra, Bryon Tjanaka, Matthew Christopher Fontaine, Aleksei Petrenko, Stefanos Nikolaidis,
 511 and Gaurav S. Sukhatme. Proximal policy gradient arborescence for quality diver-
 512 sity reinforcement learning. In *The Twelfth International Conference on Learning Representa-
 513 tions, ICLR 2024, Vienna, Austria, 2024*. URL <https://openreview.net/forum?id=TFKIfhvdmZ>.

514

515 Varun Bhatt, Bryon Tjanaka, Matthew C. Fontaine, and Stefanos Nikolaidis. Deep surrogate as-
 516 sisted generation of environments. In *Advances in Neural Information Processing Systems 35:
 517 Annual Conference on Neural Information Processing Systems 2022, NeurIPS 2022, New Or-
 518 leans, LA, USA, 2022*. URL http://papers.nips.cc/paper_files/paper/2022/hash/f649556471416b35e60ae0de7cle3619-Abstract-Conference.html.

519

520 Christopher M. Bishop. *Pattern recognition and machine learning, 5th Edition*. Information science
 521 and statistics. Springer, 2007. URL <https://www.worldcat.org/oclc/71008143>.

522

523 Raphaël Boige, Guillaume Richard, Jérémie Donà, Thomas Pierrot, and Antoine Cully. Gradient-
 524 informed quality diversity for the illumination of discrete spaces. In *Proceedings of the Genetic
 525 and Evolutionary Computation Conference, GECCO 2023, Lisbon, Portugal*, pp. 119–128. ACM,
 526 2023. URL <https://doi.org/10.1145/3583131.3590407>.

527

528 James Bradbury, Roy Frostig, Peter Hawkins, Matthew James Johnson, Chris Leary, Dougal
 529 Maclaurin, George Necula, Adam Paszke, Jake VanderPlas, Skye Wanderman-Milne, and Qiao
 530 Zhang. JAX: composable transformations of Python+NumPy programs, 2018. URL <http://github.com/jax-ml/jax>.

531

532 Herbie Bradley, Andrew Dai, Hannah Benita Teufel, Jenny Zhang, Koen Oostermeijer, Marco
 533 Bellagente, Jeff Clune, Kenneth O. Stanley, Grégory Schott, and Joel Lehman. Quality-
 534 diversity through AI feedback. In *The Twelfth International Conference on Learning Repre-
 535 sentations, ICLR*. OpenReview.net, 2024. URL <https://openreview.net/forum?id=owokKCrGYr>.

536

537 Konstantinos Chatzilygeroudis, Antoine Cully, Vassilis Vassiliades, and Jean-Baptiste Mouret.
 538 Quality-diversity optimization: a novel branch of stochastic optimization. In *Black box opti-
 539 mization, machine learning, and no-free lunch theorems*, pp. 109–135. Springer, 2021.

540 Peng Chen, Keyi Wu, Joshua Chen, Tom O’Leary-Roseberry, and Omar Ghattas. Projected
 541 stein variational newton: A fast and scalable bayesian inference method in high dimen-
 542 sions. In *Advances in Neural Information Processing Systems 32: Annual Conference*
 543 on *Neural Information Processing Systems 2019, NeurIPS 2019, Vancouver, BC, Canada*,
 544 pp. 15104–15113, 2019. URL <https://proceedings.neurips.cc/paper/2019/hash/eea5d933e9dce59c7dd0f6532f9ea81b-Abstract.html>.

545

546 Tae Jong Choi and Julian Togelius. Self-referential quality diversity through differential map-elites.
 547 In *GECCO ’21: Genetic and Evolutionary Computation Conference, Lille, France*, pp. 502–509.
 548 ACM, 2021. URL <https://doi.org/10.1145/3449639.3459383>.

549

550 Antoine Cully, Jeff Clune, Danesh Tarapore, and Jean-Baptiste Mouret. Robots that can adapt
 551 like animals. *Nat.*, 521(7553):503–507, 2015. URL <https://doi.org/10.1038/nature14422>.

552

553 Li Ding, Jenny Zhang, Jeff Clune, Lee Spector, and Joel Lehman. Quality diversity through hu-
 554 man feedback: Towards open-ended diversity-driven optimization. In *Forty-first International*
 555 *Conference on Machine Learning, ICML 2024, Vienna, Austria*. OpenReview.net, 2024. URL
 556 <https://openreview.net/forum?id=9z1ZuAAb08>.

557

558 Maxence Faldor, Félix Chalumeau, Manon Flageat, and Antoine Cully. Map-elites with descriptor-
 559 conditioned gradients and archive distillation into a single policy. In *Proceedings of the Genetic*
 560 and *Evolutionary Computation Conference, GECCO 2023, Lisbon, Portugal*, pp. 138–146. ACM,
 561 2023. URL <https://doi.org/10.1145/3583131.3590503>.

562

563 Matthew C. Fontaine and Stefanos Nikolaidis. Differentiable quality diversity. In *Advances in Neu-*
 564 *ral Information Processing Systems 34: Annual Conference on Neural Information Processing*
 565 *Systems, NeurIPS*, pp. 10040–10052, 2021. URL <https://proceedings.neurips.cc/paper/2021/hash/532923f11ac97d3e7cb0130315b067dc-Abstract.html>.

566

567 Matthew C. Fontaine and Stefanos Nikolaidis. Evaluating human-robot interaction algorithms in
 568 shared autonomy via quality diversity scenario generation. *ACM Trans. Hum. Robot Interact.*, 11
 569 (3):25:1–25:30, 2022. URL <https://doi.org/10.1145/3476412>.

570

571 Matthew C. Fontaine and Stefanos Nikolaidis. Covariance matrix adaptation map-annealing. In *Pro-*
 572 *ceedings of the Genetic and Evolutionary Computation Conference, GECCO 2023, Lisbon, Portu-*
 573 *gal*, pp. 456–465. ACM, 2023. URL <https://doi.org/10.1145/3583131.3590389>.

574

575 Matthew C. Fontaine, Scott Lee, Lisa B. Soros, Fernando de Mesentier Silva, Julian Togelius, and
 576 Amy K. Hoover. Mapping hearthstone deck spaces through map-elites with sliding boundaries. In
 577 *Proceedings of the Genetic and Evolutionary Computation Conference, GECCO 2019, Prague,*
 578 *Czech Republic*, pp. 161–169. ACM, 2019. URL <https://doi.org/10.1145/3321707.3321794>.

579

580 Matthew C. Fontaine, Julian Togelius, Stefanos Nikolaidis, and Amy K. Hoover. Covariance matrix
 581 adaptation for the rapid illumination of behavior space. In *GECCO ’20: Genetic and Evolutionary*
 582 *Computation Conference, Cancún Mexico*, pp. 94–102. ACM, 2020. URL <https://doi.org/10.1145/3377930.3390232>.

583

584 Matthew C. Fontaine, Ruilin Liu, Ahmed Khalifa, Jignesh Modi, Julian Togelius, Amy K. Hoover,
 585 and Stefanos Nikolaidis. Illuminating mario scenes in the latent space of a generative adversar-
 586 ial network. In *Thirty-Fifth AAAI Conference on Artificial Intelligence, AAAI 2021, Thirty-Third*
 587 *Conference on Innovative Applications of Artificial Intelligence, IAAI 2021, The Eleventh Sym-
 588 posium on Educational Advances in Artificial Intelligence, EAAI 2021, Virtual Event*, pp. 5922–
 589 5930. AAAI Press, 2021. URL <https://doi.org/10.1609/aaai.v35i7.16740>.

590

591 Dan Friedman and Adji Boussou Dieng. The vendi score: A diversity evaluation metric for machine
 592 learning. *Trans. Mach. Learn. Res.*, 2023. URL <https://openreview.net/forum?id=g970HbQyk1>.

593

594 Adam Gaier, Alexander Asteroth, and Jean-Baptiste Mouret. Data-efficient design exploration
 595 through surrogate-assisted illumination. *Evol. Comput.*, 26(3), 2018. URL https://doi.org/10.1162/evco_a_00231.

594 Luca Grillotti and Antoine Cully. Unsupervised behaviour discovery with quality-diversity optimi-
 595 sation. *CoRR*, abs/2106.05648, 2021. URL <https://arxiv.org/abs/2106.05648>.
 596

597 Alexander Hagg, Adam Gaier, Dominik Wilde, Alexander Asteroth, Holger Foysi, and Dirk Reith.
 598 Full domain analysis in fluid dynamics. *CoRR*, abs/2505.22275, 2025. URL <https://doi.org/10.48550/arXiv.2505.22275>.
 599

600 Saeed Hedayatian and Stefanos Nikolaidis. Autoqd: Automatic discovery of diverse behaviors with
 601 quality-diversity optimization. *CoRR*, abs/2506.05634, 2025. URL <https://doi.org/10.48550/arXiv.2506.05634>.
 602

603 Johann Huber, François Hélenon, Miranda Coninx, Faïz Ben Amar, and Stéphane Doncieux. Quality
 604 diversity under sparse reward and sparse interaction: Application to grasping in robotics. *CoRR*,
 605 abs/2308.05483, 2023. URL <https://doi.org/10.48550/arXiv.2308.05483>.
 606

607 Francisco Ibarrola and Kazjon Grace. Differentiable quality-diversity for co-creative sketching
 608 AI. In *Proceedings of the 14th International Conference on Computational Creativity, ICCC 2023, Ontario, Canada*, pp. 84–88. Association for Computational Creativity
 609 (ACC), 2023. URL https://computationalcreativity.net/iccc23/papers/ICCC-2023_paper_101.pdf.
 610

611 Gardar Ingvarsson, Mikayel Samvelyan, Bryan Lim, Manon Flageat, Antoine Cully, and Tim
 612 Rocktäschel. Mix-me: Quality-diversity for multi-agent learning. *CoRR*, abs/2311.01829, 2023.
 613 URL <https://doi.org/10.48550/arXiv.2311.01829>.
 614

615 Hannah Janmohamed, Marta Wolinska, Shikha Surana, Thomas Pierrot, Aron Walsh, and Antoine
 616 Cully. Multi-objective quality-diversity for crystal structure prediction. In *Proceedings of the
 617 Genetic and Evolutionary Computation Conference, GECCO 2024, Melbourne, VIC, Australia*.
 618 ACM, 2024. URL <https://doi.org/10.1145/3638529.3654048>.
 619

620 Tero Karras, Samuli Laine, Miika Aittala, Janne Hellsten, Jaakko Lehtinen, and Timo
 621 Aila. Analyzing and improving the image quality of stylegan. In *2020 IEEE/CVF Conference
 622 on Computer Vision and Pattern Recognition, CVPR 2020, Seattle, WA, USA*, pp. 8107–8116. Computer Vision Foundation / IEEE, 2020. URL https://openaccess.thecvf.com/content_CVPR_2020/html/Karras_Analyzing_and_Improving_the_Image_Quality_of_StyleGAN_CVPR_2020_paper.html.
 623

624 Paul Kent, Jürgen Branke, Adam Gaier, and Jean-Baptiste Mouret. A discretization-free metric for
 625 assessing quality diversity algorithms. In *GECCO '22: Genetic and Evolutionary Computation
 626 Conference, Companion Volume, Boston, Massachusetts, USA*, pp. 2131–2135. ACM, 2022. URL
 627 <https://doi.org/10.1145/3520304.3534018>.
 628

629 Diederik P. Kingma and Jimmy Ba. Adam: A method for stochastic optimization. In *3rd Inter-
 630 national Conference on Learning Representations, ICLR 2015, San Diego, CA, USA, May 7-9,
 631 2015, Conference Track Proceedings*, 2015. URL <http://arxiv.org/abs/1412.6980>.
 632

633 Joel Lehman and Kenneth O. Stanley. Evolving a diversity of virtual creatures through novelty
 634 search and local competition. In *13th Annual Genetic and Evolutionary Computation Conference,
 635 GECCO 2011, Proceedings, Dublin, Ireland*, pp. 211–218. ACM, 2011. URL <https://doi.org/10.1145/2001576.2001606>.
 636

637 Qiang Liu and Dilin Wang. Stein variational gradient descent: A general purpose bayesian
 638 inference algorithm. In *Advances in Neural Information Processing Systems 29: Annual
 639 Conference on Neural Information Processing Systems 2016, Barcelona, Spain*, pp. 2370–2378,
 640 2016. URL <https://proceedings.neurips.cc/paper/2016/hash/b3ba8f1bee1238a2f37603d90b58898d-Abstract.html>.
 641

642 Yang Liu, Prajit Ramachandran, Qiang Liu, and Jian Peng. Stein variational policy gradient. In *Pro-
 643 ceedings of the Thirty-Third Conference on Uncertainty in Artificial Intelligence, UAI 2017, Syd-
 644 ney, Australia*. AUAI Press, 2017. URL <http://auai.org/uai2017/proceedings/papers/239.pdf>.
 645

648 Jon McCormack and Camilo Cruz Gambardella. Quality-diversity for aesthetic evolution. In
 649 *Artificial Intelligence in Music, Sound, Art and Design - 11th International Conference, Evo-*
 650 *MUSART 2022, Held as Part of EvoStar 2022, Madrid, Spain, April 20-22, 2022, Proceed-*
 651 *ings*, volume 13221 of *Lecture Notes in Computer Science*, pp. 369–384. Springer, 2022. URL
 652 https://doi.org/10.1007/978-3-031-03789-4_24.

653
 654 Jean-Baptiste Mouret. Fast generation of centroids for map-elites. In *Companion Proceedings of the*
 655 *Conference on Genetic and Evolutionary Computation, GECCO 2023, Companion Volume, Lis-*
 656 *bon, Portugal*, pp. 155–158. ACM, 2023. URL <https://doi.org/10.1145/3583133.3590726>.

658 George L. Nemhauser, Laurence A. Wolsey, and Marshall L. Fisher. An analysis of approxima-
 659 tions for maximizing submodular set functions - I. *Math. Program.*, 14(1):265–294, 1978. URL
 660 <https://doi.org/10.1007/BF01588971>.

661
 662 Quan Nguyen and Adji Bousso Dieng. Quality-weighted vendi scores and their application to di-
 663 verse experimental design. In *Forty-first International Conference on Machine Learning, ICML*.
 664 OpenReview.net, 2024. URL <https://openreview.net/forum?id=gbD9MAC9p0>.

665 Olle Nilsson and Antoine Cully. Policy gradient assisted map-elites. In *GECCO '21: Genetic and*
 666 *Evolutionary Computation Conference, Lille, France*, pp. 866–875. ACM, 2021. URL <https://doi.org/10.1145/3449639.3459304>.

667
 668 Giuseppe Paolo, Alban Laflaqui  re, Alexandre Coninx, and St  phane Doncieux. Unsupervised
 669 learning and exploration of reachable outcome space. In *2020 IEEE International Conference on*
 670 *Robotics and Automation, ICRA*, pp. 2379–2385. IEEE, 2020. URL <https://doi.org/10.1109/ICRA40945.2020.9196819>.

671
 672 Thomas Pierrot, Valentin Mac  , Felix Chalumeau, Arthur Flajolet, Geoffrey Cideron, Karim Be-
 673 guir, Antoine Cully, Olivier Sigaud, and Nicolas Perrin-Gilbert. Diversity policy gradient for
 674 sample efficient quality-diversity optimization. In *Proceedings of the Genetic and Evolutionary*
 675 *Computation Conference*, pp. 1075–1083, 2022.

676
 677 Justin K. Pugh, Lisa B. Soros, and Kenneth O. Stanley. Quality diversity: A new frontier for evo-
 678 lutionary computation. *Frontiers Robotics AI*, 3:40, 2016. URL <https://doi.org/10.3389/frobt.2016.00040>.

679
 680 Chao Qian, Ke Xue, and Ren-Jian Wang. Quality-diversity algorithms can provably be helpful
 681 for optimization. In *Proceedings of the Thirty-Third International Joint Conference on Artifi-*
 682 *cial Intelligence, IJCAI*, pp. 6994–7002. ijcai.org, 2024. URL <https://www.ijcai.org/proceedings/2024/773>.

683
 684 Alec Radford, Jong Wook Kim, Chris Hallacy, Aditya Ramesh, Gabriel Goh, Sandhini Agar-
 685 wal, Girish Sastry, Amanda Askell, Pamela Mishkin, Jack Clark, Gretchen Krueger, and Ilya
 686 Sutskever. Learning transferable visual models from natural language supervision. In *Proceedings*
 687 *of the 38th International Conference on Machine Learning, ICML*, volume 139 of *Proceedings*
 688 *of Machine Learning Research*, pp. 8748–8763. PMLR, 2021. URL <http://proceedings.mlr.press/v139/radford21a.html>.

689
 690 Leonard Andreevi   Rastrigin. Systems of extremal control. *Nauka*, 1974.

691
 692 Mikayel Samvelyan, Sharath Chandra Raparthy, Andrei Lupu, Eric Hambro, Aram H.
 693 Markosyan, Manish Bhatt, Yuning Mao, Minqi Jiang, Jack Parker-Holder, Jakob N. Fo-
 694 erster, Tim Rockt  schel, and Roberta Raileanu. Rainbow teaming: Open-ended gen-
 695 eration of diverse adversarial prompts. In Amir Globersons, Lester Mackey, Danielle
 696 Belgrave, Angela Fan, Ulrich Paquet, Jakub M. Tomczak, and Cheng Zhang (eds.),
 697 *Advances in Neural Information Processing Systems 38: Annual Conference on Neu-*
 698 *ral Information Processing Systems 2024, NeurIPS 2024, Vancouver, BC, Canada*,
 699 2024. URL http://papers.nips.cc/paper_files/paper/2024/hash/8147a43d030b43a01020774ae1d3e3bb-Abstract-Conference.html.

702 Konstantinos Sfikas, Antonios Liapis, and Georgios N. Yannakakis. Controllable exploration of a
 703 design space via interactive quality diversity. In *Companion Proceedings of the Conference on*
 704 *Genetic and Evolutionary Computation, GECCO 2023, Companion Volume, Lisbon, Portugal,*
 705 pp. 167–170. ACM, 2023. URL <https://doi.org/10.1145/3583133.3590616>.

706 Yingtao Tian and David Ha. Modern evolution strategies for creativity: Fitting concrete images and
 707 abstract concepts. In *Artificial Intelligence in Music, Sound, Art and Design - 11th International*
 708 *Conference, EvoMUSART 2022, Held as Part of EvoStar 2022, Madrid, Spain, Proceedings,*
 709 volume 13221 of *Lecture Notes in Computer Science*, pp. 275–291. Springer, 2022. URL https://doi.org/10.1007/978-3-031-03789-4_18.

710 Bryon Tjanaka, Matthew C. Fontaine, David H. Lee, Aniruddha Kalkar, and Stefanos Nikolaidis.
 711 Training diverse high-dimensional controllers by scaling covariance matrix adaptation map-
 712 annealing. *IEEE Robotics Autom. Lett.*, 8(10):6771–6778, 2023a. URL <https://doi.org/10.1109/LRA.2023.3313012>.

713 Bryon Tjanaka, Matthew C. Fontaine, David H. Lee, Yulun Zhang, Nivedit Reddy Balam, Nathaniel
 714 Dennler, Sujay S. Garlanka, Nikitas Dimitri Klapsis, and Stefanos Nikolaidis. pyribs: A bare-
 715 bones python library for quality diversity optimization. In *Proceedings of the Genetic and Evo-
 716 lutionary Computation Conference, GECCO 2023, Lisbon, Portugal*, pp. 220–229. ACM, 2023b.
 717 URL <https://doi.org/10.1145/3583131.3590374>.

718 Vassilis Vassiliades, Konstantinos I. Chatzilygeroudis, and Jean-Baptiste Mouret. Using centroidal
 719 voronoi tessellations to scale up the multidimensional archive of phenotypic elites algorithm.
 720 *IEEE Trans. Evol. Comput.*, 22(4):623–630, 2018. URL <https://doi.org/10.1109/TEVC.2017.2735550>.

721 Zhenglin Wan, Xingrui Yu, David Mark Bossens, Yueming Lyu, Qing Guo, Flint Xiaofeng Fan,
 722 Yew-Soon Ong, and Ivor Tsang. Diversifying robot locomotion behaviors with extrinsic behav-
 723 ioral curiosity. In *Forty-second International Conference on Machine Learning*, 2025. URL
 724 <https://openreview.net/forum?id=sfdFOs68Ia>.

725 Dilin Wang, Ziyang Tang, Chandrajit Bajaj, and Qiang Liu. Stein variational gradient descent
 726 with matrix-valued kernels. In *Advances in Neural Information Processing Systems 32: An-
 727 nual Conference on Neural Information Processing Systems 2019, NeurIPS 2019, Vancouver,
 728 BC, Canada*, pp. 7834–7844, 2019. URL <https://proceedings.neurips.cc/paper/2019/hash/5dc0ddd3d918c70d380d32bce4e733a-Abstract.html>.

729 Ren-Jian Wang, Ke Xue, Zeyu Qin, Ziniu Li, Sheng Tang, Hao-Tian Li, Shengcui Liu, and Chao
 730 Qian. Quality-diversity red-teaming: Automated generation of high-quality and diverse attackers
 731 for large language models. *CoRR*, abs/2506.07121, 2025. URL <https://doi.org/10.48550/arXiv.2506.07121>.

732 Zhou Wang, Alan C. Bovik, Hamid R. Sheikh, and Eero P. Simoncelli. Image quality assessment:
 733 from error visibility to structural similarity. *IEEE Trans. Image Process.*, 13(4):600–612, 2004.
 734 URL <https://doi.org/10.1109/TIP.2003.819861>.

735 Xingrui Yu, Zhenglin Wan, David Mark Bossens, Yueming Lyu, Qing Guo, and Ivor W. Tsang.
 736 Imitation from diverse behaviors: Wasserstein quality diversity imitation learning with single-
 737 step archive exploration. In *Proceedings of the 24th International Conference on Autonomous*
 738 *Agents and Multiagent Systems, AAMAS 2025, Detroit, MI, USA*, pp. 2271–2280. International
 739 Foundation for Autonomous Agents and Multiagent Systems / ACM, 2025. URL <https://dl.acm.org/doi/10.5555/3709347.3743867>.

740 Tom Zahavy, Yannick Schroecker, Feryal M. P. Behbahani, Kate Baumli, Sebastian Flennerhag,
 741 Shaobo Hou, and Satinder Singh. Discovering policies with domino: Diversity optimization
 742 maintaining near optimality. In *The Eleventh International Conference on Learning Represen-
 743 tations, ICLR 2023, Kigali, Rwanda*. OpenReview.net, 2023. URL <https://openreview.net/forum?id=kjkdzbW3b8p>.

744 Marvin Zammit, Antonios Liapis, and Georgios N. Yannakakis. Map-elites with transverse as-
 745 sessment for multimodal problems in creative domains. In *Artificial Intelligence in Music,*

756 *Sound, Art and Design - 13th International Conference, EvoMUSART 2024, Held as Part of*
757 *EvoStar 2024, Aberystwyth, UK, April 3-5, 2024, Proceedings*, volume 14633 of *Lecture Notes*
758 *in Computer Science*, pp. 401–417. Springer, 2024. URL https://doi.org/10.1007/978-3-031-56992-0_26.

760 Yulun Zhang, Matthew C. Fontaine, Amy K. Hoover, and Stefanos Nikolaidis. Deep surrogate
761 assisted map-elites for automated hearthstone deckbuilding. In *GECCO '22: Genetic and Evolu-*
762 *tionary Computation Conference, Boston, Massachusetts, USA*, pp. 158–167. ACM, 2022. URL
763 <https://doi.org/10.1145/3512290.3528718>.

764 Yulun Zhang, Matthew C. Fontaine, Varun Bhatt, Stefanos Nikolaidis, and Jiaoyang Li. Arbitrarily
765 scalable environment generators via neural cellular automata (extended abstract). In *Sev-*
766 *enteenth International Symposium on Combinatorial Search, SOCS 2024, Kananaskis, Alberta,*
767 *Canada*, pp. 307–308. AAAI Press, 2024. URL <https://doi.org/10.1609/socs.v17i1.31594>.

768 Sheng Zhong, Dmitry Berenson, and Nima Fazeli. CHSEL: producing diverse plausible pose esti-
769 *mates from contact and free space data*. In *Robotics: Science and Systems XIX, Daegu, Republic*
770 *of Korea, July 10-14, 2023*, 2023. URL <https://doi.org/10.15607/RSS.2023.XIX.077>.

771 Jingwei Zhuo, Chang Liu, Jiaxin Shi, Jun Zhu, Ning Chen, and Bo Zhang. Message passing stein
772 variational gradient descent. In *Proceedings of the 35th International Conference on Machine*
773 *Learning, ICML 2018, Stockholmsmässan, Stockholm, Sweden*, volume 80 of *Proceedings of*
774 *Machine Learning Research*, pp. 6013–6022. PMLR, 2018. URL <http://proceedings.mlr.press/v80/zhuo18a.html>.

775

776

777

778

779

780

781

782

783

784

785

786

787

788

789

790

791

792

793

794

795

796

797

798

799

800

801

802

803

804

805

806

807

808

809

810 A LOWER BOUNDING SOFT QD SCORE
811812 A.1 APPROXIMATE SOFT QD SCORE
813814 Here, we will provide a formal proof of Theorem 2.
815816 Similar to the main paper, let Θ be a parameter space and $\boldsymbol{\theta} = \{\theta_1, \dots, \theta_N\}$ be a set of N solutions
817 where $\theta_n \in \Theta$. Furthermore, let $f : \Theta \rightarrow [0, \infty)$ be an objective function that assigns higher values
818 to better solutions, and let $\text{desc} : \Theta \rightarrow \mathbb{R}^d$ be the behavior descriptor function that quantifies the
819 behavior of each solution with a d -dimensional vector. Throughout the proofs, we use \mathbf{b}_i and f_i as
820 shorthands for $\text{desc}(\theta_i)$ and $f(\theta_i)$, respectively. The Soft QD Score of the population $\boldsymbol{\theta}$ is defined
821 as

822
$$S(\boldsymbol{\theta}) = \int_{\mathcal{B}} v_{\boldsymbol{\theta}}(\mathbf{b}) d\mathbf{b} = \int_{\mathcal{B}} \left[\max_{1 \leq n \leq N} f_n \exp \left(-\frac{\|\mathbf{b} - \mathbf{b}_n\|^2}{2\sigma^2} \right) \right] d\mathbf{b}. \quad (6)$$

823 **Theorem 2.** *Given a population $\boldsymbol{\theta} = \{\theta_n\}_{n=1}^N$ with qualities $\{f_n\}_{n=1}^N$ and behavior descriptor
824 vectors $\{\mathbf{b}_n\}_{n=1}^N$ in behavior space $\mathcal{B} = \mathbb{R}^d$, its Soft QD Score $S(\boldsymbol{\theta})$ can be approximated by a
825 lower bound $\tilde{S}(\boldsymbol{\theta})$ defined as:*

826
$$\tilde{S}(\boldsymbol{\theta}) = (2\pi\sigma^2)^{\frac{d}{2}} \left[\sum_{n=1}^N f_n - \sum_{1 \leq i < j \leq N} \sqrt{f_i f_j} \exp \left(-\frac{\|\mathbf{b}_i - \mathbf{b}_j\|^2}{8\sigma^2} \right) \right] \quad (7)$$

831 *Proof.* To make the notation simpler, let us define the *contribution of a single solution θ_n at a point*
832 $\mathbf{b} \in \mathcal{B}$ as

833
$$g_n(\mathbf{b}) = f_n \exp \left(-\frac{\|\mathbf{b} - \mathbf{b}_n\|^2}{2\sigma^2} \right). \quad (8)$$

835 The behavior value $v_{\boldsymbol{\theta}}(\mathbf{b})$ is the maximum of these individual contributions:

836
$$v_{\boldsymbol{\theta}}(\mathbf{b}) = \max_n g_n(\mathbf{b}) \quad (9)$$

838 Using Maximum-minimums identity, we can rewrite this as
839

840
$$v_{\boldsymbol{\theta}}(\mathbf{b}) = \max_n g_n(\mathbf{b}) \quad (10)$$

841
$$= \sum_i g_i(\mathbf{b}) - \sum_{i < j} \min(g_i(\mathbf{b}), g_j(\mathbf{b})) + \sum_{i < j < k} \min(g_i(\mathbf{b}), g_j(\mathbf{b}), g_k(\mathbf{b})) - \dots \quad (11)$$

844 Therefore,

846
$$S(\boldsymbol{\theta}) = \int \max_n g_n(\mathbf{b}) d\mathbf{b} \quad (12)$$

848
$$= \sum_i \int g_i(\mathbf{b}) d\mathbf{b} \quad (13)$$

850
$$- \sum_{i < j} \int \min(g_i(\mathbf{b}), g_j(\mathbf{b})) d\mathbf{b} \quad (14)$$

853
$$+ \sum_{i < j < k} \int \min(g_i(\mathbf{b}), g_j(\mathbf{b}), g_k(\mathbf{b})) d\mathbf{b} \quad (15)$$

855
$$- \dots \quad (16)$$

857 To get a tractable lower bound on this, we truncate the series and only consider the first two sums.
858 This discards the higher-order interactions involving three or more solutions. Intuitively, if the
859 solutions are well-spread in the behavior space (i.e., $\|\mathbf{b}_i - \mathbf{b}_j\|^2 \gg 2\sigma^2$) this approximation is
860 acceptable (detailed error analysis is provided in the next section). The second order-approximation,
861 $\tilde{S}(\boldsymbol{\theta})$, is therefore obtained by only keeping the individual and pairwise effects:

862
$$S(\boldsymbol{\theta}) \approx \tilde{S}(\boldsymbol{\theta}) = \sum_i \int g_i(\mathbf{b}) d\mathbf{b} - \sum_{i < j} \int \min(g_i(\mathbf{b}), g_j(\mathbf{b})) d\mathbf{b} \quad (17)$$

864 Next, we will derive a closed-form solution for each of the two terms.
 865

866 **The Quality Term (Individual Contributions):** The integrals in the first sum are standard Gaussian
 867 integrals and represent the contribution of each solution to the Score, irrespective of other solutions.
 868 We can evaluate them analytically:

$$869 \int_{\mathbb{R}^d} g_i(\mathbf{b}) d\mathbf{b} = \int_{\mathbb{R}^d} f_i \exp\left(-\frac{\|\mathbf{b} - \mathbf{b}_i\|^2}{2\sigma^2}\right) d\mathbf{b} = f_i (2\pi\sigma^2)^{\frac{d}{2}} \quad (18)$$

872 Hence, the first sum in $\tilde{S}(\theta)$ evaluates to

$$873 \sum_{i=1}^N \int_{\mathbb{R}^d} g_i(\mathbf{b}) d\mathbf{b} = (2\pi\sigma^2)^{\frac{d}{2}} \sum_{i=1}^N f_i. \quad (19)$$

877 **The Diversity Term (Pairwise Overlaps):** The integrals in the second term are more difficult to
 878 compute and require yet another approximation. Note that for any pair of non-negative numbers
 879 x, y we have $\min(x, y) \leq \sqrt{xy}$ (geometric mean). Using this, we have the following upper bound
 880 approximation:

$$881 \int_{\mathbb{R}^d} \min(g_i(\mathbf{b}), g_j(\mathbf{b})) d\mathbf{b} \approx \int_{\mathbb{R}^d} \sqrt{g_i(\mathbf{b})g_j(\mathbf{b})} d\mathbf{b}. \quad (20)$$

883 Now note that

$$884 \sqrt{g_i(\mathbf{b})g_j(\mathbf{b})} = \sqrt{f_i \exp\left(-\frac{\|\mathbf{b} - \mathbf{b}_i\|^2}{2\sigma^2}\right) f_j \exp\left(-\frac{\|\mathbf{b} - \mathbf{b}_j\|^2}{2\sigma^2}\right)} \quad (21)$$

$$885 = \sqrt{f_i f_j} \exp\left(-\frac{\|\mathbf{b} - \mathbf{b}_i\|^2 + \|\mathbf{b} - \mathbf{b}_j\|^2}{4\sigma^2}\right). \quad (22)$$

890 The exponent is a quadratic in \mathbf{b} and can be simplified as

$$891 \|\mathbf{b} - \mathbf{b}_i\|^2 + \|\mathbf{b} - \mathbf{b}_j\|^2 = \|\mathbf{b}\|^2 - 2\mathbf{b} \cdot \mathbf{b}_i + \|\mathbf{b}_i\|^2 + \|\mathbf{b}\|^2 - 2\mathbf{b} \cdot \mathbf{b}_j + \|\mathbf{b}_j\|^2 \quad (23)$$

$$892 = 2\|\mathbf{b}\|^2 - 2\mathbf{b} \cdot (\mathbf{b}_i + \mathbf{b}_j) + \|\mathbf{b}_i\|^2 + \|\mathbf{b}_j\|^2 \quad (24)$$

$$893 = 2 \left\| \mathbf{b} - \frac{\mathbf{b}_i + \mathbf{b}_j}{2} \right\|^2 - 2 \left\| \frac{\mathbf{b}_i + \mathbf{b}_j}{2} \right\|^2 + \|\mathbf{b}_i\|^2 + \|\mathbf{b}_j\|^2 \quad (25)$$

$$894 = 2 \left\| \mathbf{b} - \frac{\mathbf{b}_i + \mathbf{b}_j}{2} \right\|^2 + \frac{1}{2} (-\|\mathbf{b}_i\|^2 - 2\mathbf{b}_i \cdot \mathbf{b}_j - \|\mathbf{b}_j\|^2 + 2\|\mathbf{b}_i\|^2 + 2\|\mathbf{b}_j\|^2) \quad (26)$$

$$895 = 2 \left\| \mathbf{b} - \frac{\mathbf{b}_i + \mathbf{b}_j}{2} \right\|^2 + \frac{1}{2} (\|\mathbf{b}_i\|^2 - 2\mathbf{b}_i \cdot \mathbf{b}_j + \|\mathbf{b}_j\|^2) \quad (27)$$

$$896 = 2 \left\| \mathbf{b} - \frac{\mathbf{b}_i + \mathbf{b}_j}{2} \right\|^2 + \frac{1}{2} \|\mathbf{b}_i - \mathbf{b}_j\|^2. \quad (28)$$

900 Substituting this back into the exponential, we get

$$901 \exp\left(-\frac{1}{4\sigma^2} \left[2 \left\| \mathbf{b} - \frac{\mathbf{b}_i + \mathbf{b}_j}{2} \right\|^2 + \frac{1}{2} \|\mathbf{b}_i - \mathbf{b}_j\|^2 \right] \right) = \exp\left(-\frac{\|\mathbf{b}_i - \mathbf{b}_j\|^2}{8\sigma^2}\right) \exp\left(-\frac{\left\| \mathbf{b} - \frac{\mathbf{b}_i + \mathbf{b}_j}{2} \right\|^2}{2\sigma^2}\right). \quad (29)$$

902 The overlap integral is therefore

$$903 \int_{\mathbb{R}^d} \sqrt{g_i g_j} d\mathbf{b} = \sqrt{f_i f_j} \exp\left(-\frac{\|\mathbf{b}_i - \mathbf{b}_j\|^2}{8\sigma^2}\right) \int_{\mathbb{R}^d} \exp\left(-\frac{\left\| \mathbf{b} - \frac{\mathbf{b}_i + \mathbf{b}_j}{2} \right\|^2}{2\sigma^2}\right) d\mathbf{b}, \quad (30)$$

904 where the integral is now just a regular Gaussian integral centered at $\frac{\mathbf{b}_i + \mathbf{b}_j}{2}$. The whole integral thus
 905 evaluates to

$$906 \sqrt{f_i f_j} (2\pi\sigma^2)^{d/2} \exp\left(-\frac{\|\mathbf{b}_i - \mathbf{b}_j\|^2}{8\sigma^2}\right) \quad (31)$$

Putting these all together, we establish a closed form approximation (lower bound) of the archive score:

$$\tilde{S}(\boldsymbol{\theta}) = (2\pi\sigma^2)^{\frac{d}{2}} \left[\sum_{n=1}^N f_n - \sum_{1 \leq i < j \leq N} \sqrt{f_i f_j} \exp\left(-\frac{\|\mathbf{b}_i - \mathbf{b}_j\|^2}{8\sigma^2}\right) \right] \quad (32)$$

□

A.2 ANALYSIS OF APPROXIMATION ERROR

The error between the true Soft QD Score of a population and the second order approximation derived above stems from two sources: (1) the truncation of higher-order interaction in the maximum-minimums equality (Equation 17), and (2) the replacing of pairwise minimums with their geometric means in the integrals (Equation 20). We will analyze each of these errors and discuss how we can control them.

Truncation Error: The truncation error for the second order approximation is

$$\varepsilon_1 = |S(\boldsymbol{\theta}) - \tilde{S}(\boldsymbol{\theta})| \quad (33)$$

$$= \left| \int \max_n g_n(\mathbf{b}) d\mathbf{b} - \left[\sum_i \int g_i(\mathbf{b}) d\mathbf{b} - \sum_{i < j} \int \min(g_i(\mathbf{b}), g_j(\mathbf{b})) d\mathbf{b} \right] \right| \quad (34)$$

$$= \left| \sum_{i < j < k} \int \min(g_i(\mathbf{b}), g_j(\mathbf{b}), g_k(\mathbf{b})) d\mathbf{b} - \dots \right| \quad (35)$$

Lemma 1 (Bonferroni Inequalities for the Maximum). *Let $\{x_1, \dots, x_N\}$ be a set of non-negative real numbers and let $S_m = \sum_{|I|=m} \min_{i \in I} x_i$. The partial sums of the maximum-minimums equality, $P_K = \sum_{m=1}^K (-1)^{m-1} S_m$, provide alternating bounds on the maximum value:*

- If K is odd, $P_K \geq \max(x_1, \dots, x_N)$.
- If K is even, $P_K \leq \max(x_1, \dots, x_N)$.

Proof. For bounding the approximation error, we only need to use this lemma with $K = 2, 3$, which we shall prove. Without loss of generality, assume that the numbers are sorted such that $x_1 \geq x_2 \geq \dots \geq x_N \geq 0$. The contribution of x_k to the sum S_m is $\binom{k-1}{m-1} x_k$, since x_k is the minimum of a subset of m variables iff the other $m-1$ elements are all chosen from the $k-1$ elements smaller than it.

The partial sums P_K can thus be written as

$$P_K = \sum_{m=1}^K (-1)^{m-1} S_m = \sum_{k=1}^N \left[\sum_{m=1}^K (-1)^{m-1} \binom{k-1}{m-1} x_k \right]. \quad (36)$$

The inner sum is a partial sum of a binomial expansion. Therefore, using the fact that

$$\sum_{j=0}^m (-1)^j \binom{n}{j} = (-1)^m \binom{n-1}{m}, \quad (37)$$

(which follows from induction on m) we can see that the coefficient of x_k in P_K is

$$C(k, K) = \sum_{j=0}^{\min(k-1, K-1)} (-1)^j \binom{k-1}{j} = (-1)^{\min(k-1, K-1)} \binom{k-2}{\min(k-1, K-1)}. \quad (38)$$

Let us now consider the cases of $K = 2$ and $K = 3$ individually.

972 **Case $K = 2$:** Consider $P_2 = \sum_i x_i - \sum_{i < j} \min(x_i, x_j)$. For all $k \geq 2$, the coefficient of x_k in P_2
 973 is $2 - k$ and x_1 is only present once, with coefficient 1 in S_1 . Therefore, we have
 974

$$975 \quad P_2 = x_1 + \sum_{k=2}^N (2 - k)x_k. \quad (39)$$

976 Since x_k 's are all non-negative and $2 - k$ is non-positive, the sum is non-positive. Therefore,
 977

$$978 \quad P_2 \leq x_1 = \max(x_1, \dots, x_N). \quad (40)$$

981 **Case $K = 3$:** Consider $P_3 = P_2 + \sum_{i < j < k} \min(x_i, x_j, x_k)$. For all $k \geq 3$, the coefficient of x_k in
 982 P_3 is $\binom{k-2}{2} = \frac{(k-2)(k-3)}{2}$. Furthermore, x_1 is only present once, with coefficient 1 in S_1 and x_2 is
 983 present only twice, once with a +1 coefficient in S_1 and once with coefficient -1 in S_2 . Therefore,
 984 we have

$$985 \quad P_3 = x_1 + 0 \cdot x_2 + \sum_{k=3}^N \frac{(k-2)(k-3)}{2} x_k. \quad (41)$$

986 Since x_k 's are all non-negative and so are all the coefficients, the sum is non-negative. Therefore,
 987

$$988 \quad P_3 \geq x_1 = \max(x_1, \dots, x_N) \quad (42)$$

□

989 **Lemma 2** (Bounding the Truncation Error). *The truncation error ε_1 is bounded by the sum of the
 990 integrals of the third-order minimums:*

$$991 \quad \varepsilon_1 \leq \sum_{i < j < k} \int \min(g_i(\mathbf{b}), g_j(\mathbf{b}), g_k(\mathbf{b})) d\mathbf{b} \quad (43)$$

992 *Proof.* The Bonferroni inequality for $K = 2$ states that for any point \mathbf{b}

$$993 \quad \max_n g_n(\mathbf{b}) \geq \sum_i g_i(\mathbf{b}) - \sum_{i < j} \min(g_i(\mathbf{b}), g_j(\mathbf{b})). \quad (44)$$

994 Integrating this pointwise inequality over the domain of \mathbf{b} yields:

$$995 \quad S(\boldsymbol{\theta}) = \int \max_k g_n(\mathbf{b}) d\mathbf{b} \geq \int \left[\sum_i g_i(\mathbf{b}) - \sum_{i < j} \min(g_i(\mathbf{b}), g_j(\mathbf{b})) \right] d\mathbf{b} = \tilde{S}(\boldsymbol{\theta}) \quad (45)$$

996 Therefore, $\tilde{S}(\boldsymbol{\theta})$ is indeed a lower bound on $S(\boldsymbol{\theta})$ and we can write the error as $\varepsilon_1 = S(\boldsymbol{\theta}) - \tilde{S}(\boldsymbol{\theta})$.
 997 Similarly, the Bonferroni inequality for $K = 3$ states that for any point \mathbf{b}

$$998 \quad \max_n g_n(\mathbf{b}) \leq \sum_i g_i(\mathbf{b}) - \sum_{i < j} \min(g_i(\mathbf{b}), g_j(\mathbf{b})) + \sum_{i < j < k} \min(g_i(\mathbf{b}), g_j(\mathbf{b}), g_k(\mathbf{b})). \quad (46)$$

999 Integrating over the domain of \mathbf{b} yields:

$$1000 \quad S(\boldsymbol{\theta}) = \int \max_n g_n(\mathbf{b}) d\mathbf{b} \quad (47)$$

$$1001 \quad \leq \int \left[\sum_i g_i(\mathbf{b}) - \sum_{i < j} \min(g_i(\mathbf{b}), g_j(\mathbf{b})) + \sum_{i < j < k} \min(g_i(\mathbf{b}), g_j(\mathbf{b}), g_k(\mathbf{b})) \right] d\mathbf{b} \quad (48)$$

$$1002 \quad = \tilde{S}(\boldsymbol{\theta}) + \int \sum_{i < j < k} \min(g_i(\mathbf{b}), g_j(\mathbf{b}), g_k(\mathbf{b})) d\mathbf{b} \quad (49)$$

$$1003 \quad \implies S(\boldsymbol{\theta}) - \tilde{S}(\boldsymbol{\theta}) \leq \int \sum_{i < j < k} \min(g_i(\mathbf{b}), g_j(\mathbf{b}), g_k(\mathbf{b})) d\mathbf{b} \quad (50)$$

$$1004 \quad \implies \varepsilon_1 \leq \sum_{i < j < k} \int \min(g_i(\mathbf{b}), g_j(\mathbf{b}), g_k(\mathbf{b})) d\mathbf{b} \quad (51)$$

□

Given the above, we use the same technique that we used before and replace minimum with geometric mean to compute the integral. We can see that

$$\int \min(g_i(\mathbf{b}), g_j(\mathbf{b}), g_k(\mathbf{b})) d\mathbf{b} \leq \int (g_i(\mathbf{b}) \cdot g_j(\mathbf{b}) \cdot g_k(\mathbf{b}))^{\frac{1}{3}} d\mathbf{b} \quad (52)$$

$$= (f_i f_j f_k)^{\frac{1}{3}} \int \exp\left(-\frac{\|\mathbf{b} - \mathbf{b}_i\|^2 + \|\mathbf{b} - \mathbf{b}_j\|^2 + \|\mathbf{b} - \mathbf{b}_k\|^2}{6\sigma^2}\right) d\mathbf{b} \quad (53)$$

The integral is the product of three Gaussians. By completing the square, similar to the pairwise case, we can rewrite it as a Gaussian centered around $\frac{\mathbf{b}_i + \mathbf{b}_j + \mathbf{b}_k}{3}$ and a constant term. The result would be

$$\int (g_i(\mathbf{b}) \cdot g_j(\mathbf{b}) \cdot g_k(\mathbf{b}))^{\frac{1}{3}} d\mathbf{b} = (f_i f_j f_k)^{\frac{1}{3}} (3\pi\sigma^2)^{\frac{d}{2}} \exp\left(-\frac{\|\mathbf{b}_i - \mathbf{b}_j\|^2 + \|\mathbf{b}_j - \mathbf{b}_k\|^2 + \|\mathbf{b}_i - \mathbf{b}_k\|^2}{18\sigma^2}\right) \quad (54)$$

So, we have

$$\varepsilon_1 \leq \sum_{i < j < k} (f_i f_j f_k)^{\frac{1}{3}} \left(\frac{2\pi\sigma^2}{3}\right)^{\frac{d}{2}} \exp\left(-\frac{\|\mathbf{b}_i - \mathbf{b}_j\|^2 + \|\mathbf{b}_j - \mathbf{b}_k\|^2 + \|\mathbf{b}_i - \mathbf{b}_k\|^2}{18\sigma^2}\right) \quad (55)$$

From this, we conclude that if the solutions are well separated (i.e., the mean squared distance of any triplet is significantly larger than $6\sigma^2$) the error becomes negligible.

Pairwise Integral Approximation Error The pairwise integral approximation error is due to the estimation of pairwise minimums using geometric means. For every pair of solutions (i, j) this error is

$$\epsilon_{i,j} = \int_{\mathcal{B}} \left(\sqrt{g_i(\mathbf{b})g_j(\mathbf{b})} - \min(g_i(\mathbf{b}), g_j(\mathbf{b})) \right) d\mathbf{b}. \quad (56)$$

It follows from the arithmetic-geometric inequality that for every non-negative numbers x and y , $\sqrt{xy} - \min(x, y) \leq \frac{1}{2}|x - y|$. Integrating over \mathbf{b} preserves this inequality, yielding

$$\epsilon_{i,j} \leq \frac{1}{2} \int_{\mathcal{B}} |g_i(\mathbf{b}) - g_j(\mathbf{b})| d\mathbf{b}. \quad (57)$$

Note that the right hand side is just the ℓ_1 distance between the functions g_i, g_j . This distance can be further simplified by breaking down $|g_i - g_j|$ using the triangle inequality. Without loss of generality, assume that $f_j \leq f_i$, then add and subtract $f_j \exp\left(-\frac{\|\mathbf{b} - \mathbf{b}_i\|^2}{2\sigma^2}\right)$, we get

$$|g_i(\mathbf{b}) - g_j(\mathbf{b})| \leq |f_i - f_j| \exp\left(-\frac{\|\mathbf{b} - \mathbf{b}_i\|^2}{2\sigma^2}\right) + f_j \left| \exp\left(-\frac{\|\mathbf{b} - \mathbf{b}_i\|^2}{2\sigma^2}\right) - \exp\left(-\frac{\|\mathbf{b} - \mathbf{b}_j\|^2}{2\sigma^2}\right) \right| \quad (58)$$

Now, if we integrate both sides, the first term in the right hand side is just a multiple of a Gaussian integral. So we would get

$$\int |g_i(\mathbf{b}) - g_j(\mathbf{b})| d\mathbf{b} \leq (2\pi\sigma^2)^{\frac{d}{2}} \left(|f_i - f_j| + f_j \int_{\mathcal{B}} |p_i(\mathbf{b}) - p_j(\mathbf{b})| d\mathbf{b} \right), \quad (59)$$

where $p_i(\mathbf{b})$ is the pdf of a Gaussian centered at \mathbf{b}_i with covariance $\sigma^2 \mathbf{I}$. The remaining integral is twice the Total Variation distance $d_{TV}(p_i, p_j)$. Using Pinsker's inequality, we can transform it into the KL divergence between two Gaussians, which does have a closed form solution, $\frac{\|\mathbf{b}_i - \mathbf{b}_j\|^2}{2\sigma^2}$. Replacing the integral and combining everything, we arrive at the following bound for the error:

$$\epsilon_{i,j} \leq (2\pi\sigma^2)^{\frac{d}{2}} \left(|f_i - f_j| + \min(f_i, f_j) \frac{\|\mathbf{b}_i - \mathbf{b}_j\|}{\sigma} \right) \quad (60)$$

Finally, using the triangle inequality, we see that

$$\varepsilon_2 \leq (2\pi\sigma^2)^{\frac{d}{2}} \sum_{i < j \leq K} \left(|f_i - f_j| + \min(f_i, f_j) \frac{\|\mathbf{b}_i - \mathbf{b}_j\|}{\sigma} \right). \quad (61)$$

Putting both of these bounds together, a final application of triangle inequality shows that

$$|S(\boldsymbol{\theta}) - \tilde{S}(\boldsymbol{\theta})| \leq \varepsilon_1 + \varepsilon_2, \quad (62)$$

where ε_1 and ε_2 are themselves bounded by Equation 55 and Equation 61, respectively.

1080 **B PROPERTIES OF SOFT QD SCORE**
 1081

1082 Here, we will further discuss some properties of the Soft QD Score that make it a suitable measure
 1083 of quality and diversity. Theorems 3, 4, 5, and 6 formalize and prove the statement of Theorem 1 in
 1084 the main paper and show multiple properties of the Soft QD Score.
 1085

1086 Theorems 3 and 4 show that SoftQD Score is monotonic with respect to population size and qualities
 1087 of members of the population. This means that adding new solutions to a population and improving
 1088 the quality of existing ones will never decrease the SoftQD Score. We note that this is a desirable, yet
 1089 non-trivial property of a measure of quality and diversity. For instance, neither mean objective value
 1090 (as a measure of quality) nor the mean behavior distance (as a measure of diversity) of a population
 1091 are monotonic with respect to the population size; that is, adding a new solution can decrease them.
 1092

1093 Theorem 5 shows that SoftQD Score is also submodular. Being submodular is particularly conven-
 1094 ient as it implies the existence of efficient approximate algorithms for maximizing it under certain
 1095 conditions. For instance, it is well known that maximizing a submodular function subject to a cardin-
 1096 ality constraint admits a $1 - \frac{1}{e}$ approximation algorithm (Nemhauser et al., 1978). This is valuable
 1097 when we want to select a fixed-size subset of a large population that preserves as much of the Soft
 1098 QD Score as possible (e.g., for evaluation or compression).
 1099

1100 Lastly, we establish a connection between the traditional QD Score and the limiting behavior of the
 1101 Soft QD Score through Theorem 6.
 1102

1103 **Theorem 3** (Monotonicity with respect to population size). *Let $\theta = \{\theta_1, \dots, \theta_N\}$ be a population
 1104 and let θ_{N+1} be any new solution. If $\theta^+ = \theta \cup \{\theta_{N+1}\}$, then $S(\theta) \leq S(\theta^+)$.*
 1105

1106 *Proof.* Let $f_{N+1} = f(\theta_{N+1})$ and $\mathbf{b}_{N+1} = \text{desc}(\theta_{N+1})$. The behavior value for the new population
 1107 θ^+ can be written as
 1108

$$v_{\theta^+}(\mathbf{b}) = \max \left(v_{\theta}(\mathbf{b}), f_{N+1} \exp \left(-\frac{\|\mathbf{b} - \mathbf{b}_{N+1}\|^2}{2\sigma^2} \right) \right) \geq v_{\theta}(\mathbf{b}). \quad (63)$$

1109 Integrating both sides of the above inequality over the behavior space \mathcal{B} yields the result:
 1110

$$S(\theta^+) = \int_{\mathcal{B}} v_{\theta^+}(\mathbf{b}) d\mathbf{b} \geq \int_{\mathcal{B}} v_{\theta}(\mathbf{b}) d\mathbf{b} = S(\theta). \quad (64)$$

1112 \square

1113 **Theorem 4** (Monotonicity with respect to quality). *Let $\theta = \{\theta_1, \dots, \theta_N\}$ be a population and
 1114 $\theta' = \theta \cup \{\theta'_n\} \setminus \{\theta_n\}$ be another population that is identical to θ except that the n -th solution θ_n
 1115 is replaced by θ'_n such that $\text{desc}(\theta) = \text{desc}(\theta') = \mathbf{b}_n$ and $f(\theta'_n) = f'_n \geq f_n = f(\theta_n)$. Then,
 1116 $S(\theta) \leq S(\theta')$.*
 1117

1118 *Proof.* Let the behavior values for θ and θ' be $v_{\theta}(\mathbf{b})$ and $v_{\theta'}(\mathbf{b})$, respectively. Since, $f'_n \geq f_n$, for
 1119 every \mathbf{b} we have $f'_n \exp(-\frac{\|\mathbf{b} - \mathbf{b}_n\|^2}{2\sigma^2}) \geq f_n \exp(-\frac{\|\mathbf{b} - \mathbf{b}_n\|^2}{2\sigma^2})$. Therefore, we can write
 1120

$$v_{\theta'}(\mathbf{b}) = \max \left(v_{\theta}(\mathbf{b}), f'_n \exp \left(-\frac{\|\mathbf{b} - \mathbf{b}_n\|^2}{2\sigma^2} \right) \right) \geq v_{\theta}(\mathbf{b}). \quad (65)$$

1121 Integrating both sides of the above inequality yields the result:
 1122

$$S(\theta') = \int_{\mathcal{B}} v_{\theta'}(\mathbf{b}) d\mathbf{b} \geq \int_{\mathcal{B}} v_{\theta}(\mathbf{b}) d\mathbf{b} = S(\theta). \quad (66)$$

1123 \square

1124 **Theorem 5** (Submodularity). *Let $\theta = \{\theta_1, \dots, \theta_N\}$ be a population. The Soft QD Score S defined
 1125 on subsets of θ is submodular. That is, for any $U \subseteq V \subseteq \theta$ and any new solution $\theta' \notin V$ with
 1126 quality $f' = f(\theta')$ and behavior vector $\mathbf{b}' = \text{desc}(\theta')$,*
 1127

$$S(U \cup \{\theta'\}) - S(U) \geq S(V \cup \{\theta'\}) - S(V). \quad (67)$$

1134 *Proof.* For brevity, let us denote $U \cup \{\theta'\}$ as U' and $V \cup \{\theta'\}$ as V' . Similar to the argument in
 1135 Theorem 3, we have

$$1137 \quad v_{U'}(\mathbf{b}) - v_U(\mathbf{b}) = \max \left(v_U(\mathbf{b}), f' \exp \left(-\frac{\|\mathbf{b} - \mathbf{b}'\|^2}{2\sigma^2} \right) \right) - v_U(\mathbf{b}) \quad (68)$$

$$1139 \quad = \max \left(0, f' \exp \left(-\frac{\|\mathbf{b} - \mathbf{b}'\|^2}{2\sigma^2} \right) - v_U(\mathbf{b}) \right). \quad (69)$$

1142 Similarly, we also have

$$1143 \quad v_{V'}(\mathbf{b}) - v_V(\mathbf{b}) = \max \left(0, f' \exp \left(-\frac{\|\mathbf{b} - \mathbf{b}'\|^2}{2\sigma^2} \right) - v_V(\mathbf{b}) \right). \quad (70)$$

1146 Since $U \subseteq V$, for every \mathbf{b} we have $v_U(\mathbf{b}) \leq v_V(\mathbf{b})$. Therefore,

$$1148 \quad v_{U'}(\mathbf{b}) - v_U(\mathbf{b}) \geq v_{V'}(\mathbf{b}) - v_V(\mathbf{b}) \quad (71)$$

1149 Integrating both sides yields the result

$$1151 \quad S(U') - S(U) \geq S(V') - S(V). \quad (72)$$

1153 \square

1154 **Theorem 6.** Let $\theta = \{\theta_1, \dots, \theta_N\}$ be a population of N solutions with corresponding quality
 1155 values f_1, \dots, f_N and distinct behaviors $\mathbf{b}_1, \dots, \mathbf{b}_N$ in \mathbb{R}^d . Let $S(\theta)$ be the Soft QD Score defines
 1156 as

$$1157 \quad S(\theta) = \int_{\mathbb{R}^d} \max_{1 \leq n \leq N} \left[f_n \exp \left(-\frac{\|\mathbf{b} - \mathbf{b}_n\|^2}{2\sigma^2} \right) \right] d\mathbf{b} \quad (73)$$

1159 In the limit as the kernel width σ approaches zero, the scaled Soft QD Score converges to the sum of
 1160 the qualities of all solutions in the population.

$$1162 \quad \lim_{\sigma \rightarrow 0} \frac{S(\theta)}{(2\pi\sigma^2)^{\frac{d}{2}}} = \sum_{n=1}^N f_n \quad (74)$$

1165 This limit is equivalent to the traditional QD Score calculated on a grid fine enough to isolate each
 1166 solution into its own cell.

1168 *Proof.* Let the scaled Soft QD Score be denoted by $L(\sigma)$:

$$1170 \quad L(\sigma) = \frac{S(\theta)}{(2\pi\sigma^2)^{\frac{d}{2}}} = \frac{1}{(2\pi\sigma^2)^{\frac{d}{2}}} \int_{\mathbb{R}^d} \max_{1 \leq n \leq N} \left[f_n \exp \left(-\frac{\|\mathbf{b} - \mathbf{b}_n\|^2}{2\sigma^2} \right) \right] d\mathbf{b} \quad (75)$$

1173 Since the sum of a set of non-negative number is at least as large as their maximum, we can replace
 1174 the max in the integral with a summation and write

$$1175 \quad L(\sigma) \leq \frac{1}{(2\pi\sigma^2)^{\frac{d}{2}}} \int_{\mathbb{R}^d} \sum_{n=1}^N \left[f_n \exp \left(-\frac{\|\mathbf{b} - \mathbf{b}_n\|^2}{2\sigma^2} \right) \right] d\mathbf{b} \quad (76)$$

$$1178 \quad = \frac{1}{(2\pi\sigma^2)^{\frac{d}{2}}} \sum_{n=1}^N f_n \int_{\mathbb{R}^d} \exp \left(-\frac{\|\mathbf{b} - \mathbf{b}_n\|^2}{2\sigma^2} \right) d\mathbf{b} \quad (77)$$

$$1181 \quad = \sum_{n=1}^N f_n. \quad (78)$$

1184 Note that Eq. 77 holds due to the linearity of integration and Eq. 78 is true since the Gaussian
 1185 integrals over the entire domain evaluate to $(2\pi\sigma^2)^{\frac{d}{2}}$.

1186 Next, let $r = \frac{1}{2} \min_{i \neq j} \|\mathbf{b}_i - \mathbf{b}_j\|$. Following this definition, we can see that the open balls $B_n =$
 1187 $\{\mathbf{b} : \|\mathbf{b} - \mathbf{b}_n\| < r\}$ centered at each behavior point with radius r are disjoint.

1188 The integrand in $S(\boldsymbol{\theta})$ is non-negative, so the integral over \mathbb{R}^d is greater than or equal to the integral
 1189 over the union of these disjoint balls:

$$1190 \quad S(\boldsymbol{\theta}) \geq \int_{\bigcup_n B_n} \max_i \left[f_i \exp \left(-\frac{\|\mathbf{b} - \mathbf{b}_i\|^2}{2\sigma^2} \right) \right] d\mathbf{b} \quad (79)$$

$$1191 \quad = \sum_n \int_{B_n} \max_i \left[f_i \exp \left(-\frac{\|\mathbf{b} - \mathbf{b}_i\|^2}{2\sigma^2} \right) \right] d\mathbf{b} \quad (80)$$

1192 For any point \mathbf{b} inside a specific ball B_n , the maximum value is always greater than or equal to the
 1193 term for n :

$$1194 \quad \max_i \left[f_i \exp \left(-\frac{\|\mathbf{b} - \mathbf{b}_i\|^2}{2\sigma^2} \right) \right] \geq f_n \exp \left(-\frac{\|\mathbf{b} - \mathbf{b}_n\|^2}{2\sigma^2} \right) \quad (81)$$

1195 Substituting this, gives a lower bound for $S(\boldsymbol{\theta})$

$$1196 \quad S(\boldsymbol{\theta}) \geq \sum_n f_n \int_{B_n} \exp \left(-\frac{\|\mathbf{b} - \mathbf{b}_n\|^2}{2\sigma^2} \right) d\mathbf{b} \quad (82)$$

1197 Now, we can analyze the limit of the scaled version of this lower bound:

$$1198 \quad \lim_{\sigma \rightarrow 0} L(\sigma) \geq \lim_{\sigma \rightarrow 0} \sum_n \frac{f_n}{(2\pi\sigma^2)^{\frac{d}{2}}} \int_{B_n} \exp \left(-\frac{\|\mathbf{b} - \mathbf{b}_n\|^2}{2\sigma^2} \right) d\mathbf{b} \quad (83)$$

$$1199 \quad = \sum_n f_n \left(\lim_{\sigma \rightarrow 0} \frac{1}{(2\pi\sigma^2)^{\frac{d}{2}}} \int_{B_n} \exp \left(-\frac{\|\mathbf{b} - \mathbf{b}_n\|^2}{2\sigma^2} \right) d\mathbf{b} \right) \quad (84)$$

1200 Similar to the integral of Eq. 77, The term in the parenthesis here is the integral of the PDF of
 1201 $\mathcal{N}(\mathbf{b}_n, \sigma^2 I)$. Since the ball B_n is a fixed region containing the mean \mathbf{b}_n , all of the probability mass
 1202 concentrates inside B_n as $\sigma \rightarrow 0$. Therefore, the limit of the integral approaches the denominator
 1203 and the whole limit will evaluate to one and we have

$$1204 \quad \lim_{\sigma \rightarrow 0} L(\sigma) \geq \sum_n f_n \quad (85)$$

1205 Together, Eq. 85 and Eq. 76 sandwich $L(\sigma)$. Hence,

$$1206 \quad \lim_{\sigma \rightarrow 0} L(\sigma) = \sum_{n=1}^N f_n. \quad (86)$$

1207 Lastly, note that if the solutions in $\boldsymbol{\theta}$ all fall into distinct cells of an archive, as is the case with
 1208 the populations that conventional QD methods generate or in the limit of having very fine-grained
 1209 archives, the sum of the objectives coincides with the QD Score and we have

$$1210 \quad \lim_{\sigma \rightarrow 0} \frac{S(\boldsymbol{\theta})}{(2\pi\sigma^2)^{\frac{d}{2}}} = \sum_{n=1}^N f_n = \text{QD Score}(\boldsymbol{\theta}) \quad (87)$$

1211 \square

1212 C ADDITIONAL ABLATIONS

1213 C.1 EFFECT OF BATCH SIZE

1214 SQUAD updates the solutions in its population one batch at a time (Section 4), primarily to reduce
 1215 the computational cost of simultaneous updates. To examine the role of batch size M , we performed
 1216 an ablation in the IC domain, evaluating SQUAD with $M \in \{4, 8, 16, 32, 64\}$. Each setting was
 1217 repeated three times with different random seeds. The results are reported in Table 3.

1218 Overall, the performance of SQUAD is stable across all tested batch sizes. Smaller batch sizes tend
 1219 to yield slightly higher QD scores, whereas larger batch sizes achieve marginally better QVS. How-
 1220 ever, these differences are minor compared to the variation observed between algorithms, indicating
 1221 that SQUAD is robust to the choice of batch size. All experiments were conducted on a machine
 1222 equipped with an NVIDIA GeForce RTX 4090. The approximate runtimes for different batch sizes
 1223 were as follows: batch size 4 took 5 hours and 47 minutes, batch size 8 took 2 hours and 55 minutes,
 1224 batch size 16 took 2 hours and 42 minutes, batch size 32 took 3 hours and 10 minutes, batch size 64
 1225 took 3 hours and 10 minutes.

1242 Table 3: **Effect of batch size on SQuAD.** Results report the mean and standard error over three
 1243 random seeds for five batch sizes. Experiment in the main paper use $M = 64$.
 1244

| Algorithm | QD Score ($\times 10^3$) | QVS |
|--------------------|----------------------------|--------------------|
| SQuAD ($M = 4$) | 5.32 ± 0.05 | 457.4 ± 0.4 |
| SQuAD ($M = 8$) | 5.12 ± 0.04 | 457.7 ± 0.4 |
| SQuAD ($M = 16$) | 5.04 ± 0.16 | 458.4 ± 0.5 |
| SQuAD ($M = 32$) | 4.99 ± 0.09 | 457.9 ± 0.3 |
| SQuAD ($M = 64$) | 5.07 ± 0.05 | 457.4 ± 0.1 |

C.2 EFFECT OF NUMBER OF NEIGHBORS

We ablate the sensitivity of SQuAD to the number of nearest neighbors k used in the diversity term of the objective. Experiments were run in the IC domain with $k \in \{0, 4, 8, 16, 32\}$ and the results over three random seeds are reported in Table 4. Note that the case $k = 0$ removes the diversity term entirely and therefore corresponds to independently optimizing each solution for quality alone.

1255 Table 4: **Effect of nearest neighbors' count on SQuAD.** Results report the mean and standard
 1256 error over three random seeds. Experiment in the main paper use $k = 16$.
 1257

| Algorithm | QD Score ($\times 10^3$) | QVS |
|--------------------|----------------------------|--------------------|
| SQuAD ($k = 0$) | 0.09 ± 0.00 | 90.8 ± 0.0 |
| SQuAD ($k = 4$) | 5.37 ± 0.06 | 457.7 ± 0.4 |
| SQuAD ($k = 8$) | 5.02 ± 0.03 | 459.7 ± 0.5 |
| SQuAD ($k = 16$) | 5.07 ± 0.05 | 457.4 ± 0.1 |
| SQuAD ($k = 32$) | 5.19 ± 0.04 | 448.5 ± 0.6 |

Two conclusions follow from these results. First, the diversity term is essential as the $k = 0$ baseline achieves significantly worse performance in both QD Score and QVS, suggesting a collapse into a set of nearly identical solutions. Second, for other values of $k > 0$, the performance is largely insensitive to the exact number of neighbors, since neither QD Score nor QVS vary largely across $k = 4, 8, 16, 32$. In practice, this means that a small k already provides the repulsive pressure needed to encourage diverse and high quality solutions.

Our hypothesis for this observed insensitivity is that once solutions are separated by distances larger than the kernel bandwidth γ , which could happen early in the optimization, the kernel contribution from farther solutions rapidly decays towards zero, so only the closest neighbors exert meaningful repulsion. This hypothesis, combined with our results indicating the important role that γ plays, also suggests several promising directions for future work: (1) per-solution or adaptive kernel widths γ based on the current spread of solutions in the behavior space to control the repulsive force each solution receives; possibly combined with (2) annealing schedules that dampen the diversity term over training so that exploration is encouraged early on and fine-grained quality optimization dominates later.

C.3 EFFECT OF BEHAVIOR SPACE TRANSFORMATION

Recall that the derivation of SQuAD's objective (Equation 5) assumed that the behavior space is unbounded. To transform the bounded behavior space $[0, 1]^d$ that is used in the tasks to \mathbb{R}^d , SQuAD used the logit transformation:

$$\mathbf{b}' = \log \frac{\mathbf{b}}{1 - \mathbf{b}}, \quad (88)$$

where all operations are performed element-wise. In our final ablation, we seek to understand the impact of this transformation on SQuAD's performance. To this end, we run SQuAD without using this transformation with three different random seeds and compare the results with the original experiments that were conducted in Section 5.3 (conducted over ten random seeds). As the comparison of the results in Table 5 shows, the logit transformation is critical to the successful performance of SQuAD.

1296 Table 5: **Effect of behavior space transformation on SQuAD.** Results report the mean and stan-
 1297 dard error over three random seeds for the ablated version and over ten random seeds for the base
 1298 version.

| Algorithm | QD Score ($\times 10^3$) | QVS |
|-------------------------------------------|----------------------------|-----------------|
| SQuAD | 5.09 ± 0.05 | 457.3 ± 0.2 |
| SQuAD (w/o behavior space transformation) | 2.96 ± 0.04 | 186.6 ± 0.8 |

1304 C.4 EFFECT OF POPULATION SIZE

1307 We also study the impact that role that population size has on the performance of SQuAD. To this
 1308 end, we compare the performance of SQuAD in the IC domain with 4 different population sizes
 1309 $N = 128, 256, 512, 1024$. The results, reported in Table 6, conform with our expectation that larger
 1310 populations yield better performance. Furthermore, we observed that the runtime of SQuAD had a
 1311 linear relation with the population size, with the mean runtimes being 24, 48, 95, 190 minutes for
 1312 population sizes of 128, 256, 512, and 1024, respectively (averaged over 3 seeds, with variances less
 1313 than 10 seconds).

1314 Table 6: **Effect of population size on SQuAD.** Results report the mean and standard error over
 1315 three random seeds. Experiment in the main paper use $N = 1024$.

| Algorithm | QD Score ($\times 10^3$) | QVS |
|----------------------|-----------------------------------|-----------------------------------|
| SQuAD ($N = 128$) | 3.24 ± 0.43 | 390.6 ± 1.6 |
| SQuAD ($N = 256$) | 4.12 ± 0.57 | 422.7 ± 0.8 |
| SQuAD ($N = 512$) | 4.26 ± 0.60 | 445.2 ± 0.3 |
| SQuAD ($N = 1024$) | 4.50 ± 0.62 | 457.5 ± 0.6 |

1322 D IMPLEMENTATION DETAILS

1323 D.1 BENCHMARK DOMAINS

1326 D.1.1 LINEAR PROJECTION

1328 We adopt the Linear Projection (LP) domain introduced by Fontaine et al. (2020), using the Rastrigin
 1329 objective function (Rastrigin, 1974). The QD search is performed over solution vectors $\mathbf{x} \in \mathbb{R}^n$,
 1330 with dimensionality set to $n = 1024$. The Rastrigin function is defined as

$$1331 \quad f_{\text{Rastrigin}}(\mathbf{x}) = 10n + \sum_{i=1}^n [x_i^2 - 10 \cos(2\pi x_i)]. \quad (89)$$

1334 Following prior work (Fontaine et al., 2019), we restrict the search space to $[-5.12, 5.12]^n$ and
 1335 apply an offset so that the global optimum is shifted from the origin to $\underbrace{[2.048, \dots, 2.048]}_n^T$. To
 1336 transform the problem from minimization to maximization, we normalize the objective via a linear
 1337 transformation

$$1339 \quad f(\mathbf{x}) = 100 \times \frac{M - f_{\text{Rastrigin}}(\mathbf{x})}{M} \quad (90)$$

1341 where M denotes the maximum value of the Rastrigin function in the search domain. This results
 1342 in objective values scaled to the range $[0, 100]$. A heatmap of the transformed Rastrigin function in
 1343 2 dimensions is depicted in Figure 5.

1344 The behavior space is defined by partitioning $\mathbf{x} = [x_1, \dots, x_n]^T$ into d equal-sized chunks and com-
 1345 puting the mean of clipped values within each chunk. More formally, the k -dimensional behavior
 1346 descriptor is given by

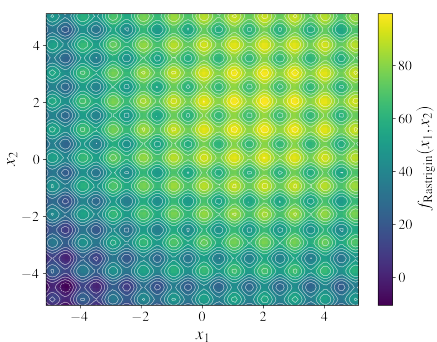
$$1347 \quad \text{desc}(\mathbf{x}) = \frac{1}{d} \left(\sum_{i=1}^{\frac{n}{d}} \text{clip}(x_i), \sum_{i=\frac{n}{d}+1}^{\frac{2n}{d}} \text{clip}(x_i), \dots, \sum_{i=\frac{(d-1)n}{d}+1}^n \text{clip}(x_i) \right)^T, \quad (91)$$

1350 where the clipping function is defined as
 1351

$$\text{clip}(x_i) = \begin{cases} x_i & \text{if } -5.12 \leq x_i \leq 5.12 \\ 5.12 & \text{otherwise} \\ x_i & \end{cases} \quad (92)$$

1355 In our experiments, we evaluated behavior spaces of dimensionality $d \in \{4, 8, 16\}$. For additional
 1356 details on this domain, including its challenges in high-dimensional settings, we refer the reader to
 1357 Fontaine & Nikolaidis (2021; 2023).
 1358

1359 D.1.2 IMAGE COMPOSITION



1362 (a) (Transformed) 2-d Rastrigin function
 1363
 1364
 1365
 1366
 1367
 1368
 1369
 1370
 1371
 1372



1373 (b) Target image for the IC domain
 1374
 1375

Figure 5

1376 Image Composition (IC) is a new differentiable QD benchmark we introduce, inspired by related
 1377 works (Tian & Ha, 2022; Ibarrola & Grace, 2023). The IC task aims to reconstruct a target image
 1378 by composing a large number of simple primitives (circles) on a canvas. The objective is to match
 1379 the target as closely as possible while exploring diverse visual effects, which are captured through
 1380 five behavioral descriptors. In this task, a solution is a vector of size $n \times 7$, where n denotes the
 1381 number of circles (here $n = 1024$). Each row parameterizes a circle with 7 values: the (x, y) center
 1382 coordinates, radius, RGB color values, and an opacity coefficient. All parameters are represented
 1383 as unconstrained logits, which are passed through sigmoidal transformations and rescaled to the
 1384 appropriate range.

1385 A differentiable renderer composites these circles in sequence onto a canvas of resolution 64×64 .
 1386 Each circle is drawn with smooth edges, controlled by a softness hyperparameter (here set to 10.0).
 1387 Rendering is performed by alpha-compositing onto a black canvas.

1388 The objective is defined as the similarity between the rendered image and a fixed target image. We
 1389 use structural similarity (SSIM) (Wang et al., 2004), normalized to the range $[0, 100]$ to measure this.
 1390 The behavioral descriptors are five statistics computed from the circles:

- 1392 • mean radius of circles,
- 1393 • variance of radii,
- 1394 • variety of RGB values in the palette (color spread),
- 1395 • coherence of circle hues in HSV space (color harmony),
- 1396 • degree of spatial clustering based on average 5-nearest-neighbor distances.

1400 These descriptors are each normalized to lie in $[0, 1]$, with higher values representing larger radii,
 1401 greater diversity, more harmony, or tighter clustering, respectively. Together with the objective, they
 1402 define a continuous and differentiable QD landscape. As the target image in our experiments, we use
 1403 Johannes Vermeer's painting Girl with a Pearl Earring (Figure 5), obtained from the freely available
 reproduction on Wikimedia Commons.

1404 D.1.3 LATENT SPACE ILLUMINATION
1405

1406 Latent Space Illumination (LSI) (Fontaine et al., 2021; Fontaine & Nikolaidis, 2021) is a challenging
1407 QD benchmark designed to illuminate the latent space of a generative model by discovering diverse
1408 and high-quality solutions. Following the experimental setup of Fontaine & Nikolaidis (2023);
1409 Tjanaka et al. (2023b), we employ StyleGAN2 Karras et al. (2020) as the generative model and use
1410 CLIP (Radford et al., 2021) to define both the objective and behavior descriptor functions.

1411 Each solution in LSI is represented as a 9216-dimensional vector corresponding to a point in the
1412 latent space of StyleGAN2. To evaluate solution quality, we pass the vector through StyleGAN2
1413 to generate an image, which is then compared to a target text prompt using CLIP embeddings.
1414 Behavior descriptors are similarly computed by comparing the generated image against pairs of
1415 descriptor sentences, one positive and one negative. Our implementation is based on JAX (Bradbury
1416 et al., 2018), and we rely on publicly available JAX-based implementations of both StyleGAN2 and
1417 CLIP.

1418 We define two task variants:

- 1419 • **Base version.** This setup follows Fontaine & Nikolaidis (2023) and uses the prompt “A
1420 photo of Tom Cruise” as the objective. Behavior descriptors are specified by two sentence
1421 pairs:
 - 1422 – (“Photo of Tom Cruise as a small child”, “Photo of Tom Cruise as an elderly person”)
 - 1423 – (“Photo of Tom Cruise with long hair”, “Photo of Tom Cruise with short hair”)
- 1424 • **Hard version.** To increase task difficulty, we use the objective prompt “A photo of a
1425 detective from a noir film” and define seven behavior descriptor pairs:
 - 1426 – (“Photo of a young kid”, “Photo of an elderly person”)
 - 1427 – (“Photo of a person with long hair”, “Photo of a person with short hair”)
 - 1428 – (“Photo of a person with dark hair”, “Photo of a person with white hair”)
 - 1429 – (“Photo of a person smiling”, “Photo of a person frowning”)
 - 1430 – (“Photo of a person with a round face”, “Photo of a person with an oval face”)
 - 1431 – (“Photo of a person with thin, sparse hair”, “Photo of a person with thick, full hair”)
 - 1432 – (“Photo of a person looking directly into the camera”, “Photo of a person looking
1433 sideways”)

1435 D.2 EVALUATION METRICS
1436

1437 We used multiple evaluation metrics in our experiments, which we shall explain here in more detail.

1438 **Vendi Score** (Friedman & Dieng, 2023) is a widely applicable metric of diversity in machine learning.
1439 Given a set of samples and a pairwise similarity function, Vendi Score can be interpreted as the
1440 effective number of unique elements in the set. Formally, it is defined as
1441

$$1442 \text{VS}(\mathbf{K}) = \exp \left(-\text{tr} \left(\frac{1}{n} \mathbf{K} \log \frac{1}{n} \mathbf{K} \right) \right) = \exp \left(-\sum_{i=1}^n \lambda_i \log \lambda_i \right), \quad (93)$$

1443 where $\mathbf{K} \in \mathbb{R}^{n \times n}$ is a positive semi-definite similarity matrix and λ_i are the eigenvalues of $\frac{1}{n} \mathbf{K}$. In
1444 our case, the similarity matrix is derived by applying the Gaussian kernel on the distance between
1445 the behavior descriptors of solutions. That is, for solutions i and j with behavior descriptors $\mathbf{b}_i, \mathbf{b}_j$
1446 we define: $\mathbf{K}_{ij} = \exp \left(-\frac{\|\mathbf{b}_i - \mathbf{b}_j\|^2}{\sigma_v^2} \right)$ where σ_v is a kernel bandwidth. For a d dimensional behavior
1447 space, we choose $\sigma_v^2 = \frac{d}{6}$ in our evaluations. This (heuristic) choice is motivated by the fact that
1448 the mean squared distance between two uniformly selected vectors in $[0, 1]^d$ is $\frac{d}{6}$. Since in all of
1449 our experiments the behavior space is defined as $[0, 1]^d$, this ensures that the similarity between two
1450 random vectors in the behavior space will be $e^{-1} \approx 0.37$.

1451 **Quality-weighted Vendi Score (QVS)** (Nguyen & Dieng, 2024) extends Vendi Score to also incor-
1452 porate the quality of solutions. It is computed by multiplying the Vendi Score by the mean quality
1453 of the solutions:

$$1454 \text{QVS}(\mathbf{K}, (f_1, \dots, f_n)) = \frac{1}{n} \sum_{i=1}^n f_i \text{VS}(\mathbf{K}), \quad (94)$$

1458 where f_i is the quality of the i -th solutions. We use QVS to capture the joint effect of quality and
 1459 diversity in a population. Importantly, the mean quality of the solutions must be non-negative for
 1460 the metric to be meaningful. While in our domains the objectives are normalized such that sensible
 1461 solutions have objectives in the $[0, 100]$ range, it is still possible for out-of-bound solutions in the
 1462 LP and LSI domains to obtain negative values, since, theoretically, their objective functions are
 1463 unbounded from below. In cases where the mean objective of the solutions were negative (which
 1464 only happened with Sep-CMA-MAE and GA-ME in LSI), we report the QVS as 0.0 and report the
 1465 fine-grained statistics, including the mean objective and Vendi Score, in Appendix E.

1466 We also leverage a discretization of the behavior space using CVT (Vassiliades et al., 2018) and
 1467 report traditional QD metrics such as **QD Score** (Pugh et al., 2016) and **Coverage**. Even though
 1468 the exponentially growing volume of the cells hinders the performance of optimization algorithms
 1469 that leverage such archives (as noted in the paper), we can still use them for evaluation. To compute
 1470 these metrics, we discretize the behavior space into a fixed number of cells (1024 for IC and 512 for
 1471 LP and LSI) and insert the solutions from a population into the resulting archive, keeping only the
 1472 best solution that lands in a cell. The **Coverage** is then defined as the fraction of cells that are filled
 1473 with solutions and captures the diversity of the population. In a same manner **QD Score** is defined
 1474 as the sum of the qualities (objectives) of all the solutions in the resulting archive, and captures both
 1475 quality and diversity.

1476 Lastly, we also use **Mean Objective** and **Max Objective** to measure the quality of populations.
 1477 These are simply defined as the mean (and respectively maximum) of the qualities (objectives) of
 1478 the solutions in a population.

1479 D.3 HYPERPARAMETERS

1481 The full set of hyperparameters that we used for the experiments can be found in the accompanying
 1482 code. Here, we will go over the most important choices.

1484 D.3.1 BASELINES

1486 All baselines use a CVT archive with 10^4 cells in LP and IC domains and a finer archive with 4×10^4
 1487 cells in the LSI domain. In LP and IC domains we ran a grid search for each algorithm on the most
 1488 important hyperparameters and selected the configuration that yielded the highest QD Score.

- 1489 • For CMA-MEGA, we searched over initial step size of the ES (σ_0) and the optimizer learning
 1490 rate.
- 1491 • For CMA-MAEGA we searched over initial step size of the ES (σ_0), optimizer learning
 1492 rate, and archive learning rate.
- 1493 • For Sep-CMA-MAE we searched over initial step size of the ES (σ_0) and archive learning
 1494 rate.
- 1495 • For GA-ME we tuned iso and line sigma parameters and the gradient step size.

1497 For LSI, we used the default hyperparameters from Fontaine & Nikolaidis (2023) used in the pyribs
 1498 (Tjanaka et al., 2023b) implementation, with the only difference being the batch size, where we use
 1499 16 instead of 32 due to computational constraints. Furthermore, for DNS, we ran a similar grid
 1500 search over the iso and line sigma parameters, the number of nearest neighbors (k), as well as the
 1501 learning rate (for the DNS-G variant) in the IC domain to determine appropriate hyperparameters.
 1502 We also chose the number of iterations such that all algorithms use (roughly) the same number of
 1503 solution evaluations.

1504 D.3.2 SQUAD

1506 By default, SQuAD uses the values presented in Table 7 for its hyperparameters and uses Adam
 1507 (Kingma & Ba, 2015) to optimize its objective. Below, we will discuss the exceptions to these
 1508 default values.

- 1509 1. **LSI domain:** Due to computational constraints, we use a population size of 256 and a
 1510 batch size of 8. We use $\gamma^2 = 0.01$ for the base version of the task and $\gamma^2 = 0.1$ for the
 1511 hard version. We also use a larger learning rate of 0.1 for the Adam optimizer.

1512 2. **LP domain:** We use $\gamma^2 = 0.1$ for the easy version, $\gamma^2 = 0.5$ for the medium version, and
 1513 $\gamma^2 = 1.0$ for the hard version.
 1514

1515 Table 7: Default SQuAD parameters

| 1516 Parameter | 1517 Value |
|-----------------------------------------|----------------------|
| 1518 Population Size (N) | 1519 1024 |
| 1519 Batch Size (M) | 1520 64 |
| 1520 No. Neighbors (K) | 1521 16 |
| 1521 Learning Rate | 0.05 |

1522 We train SQuAD for 1000 iterations in LP and IC and for 175 iterations in LSI. The number of
 1523 training iterations of baselines were set such that they use at least as many evaluations as SQuAD
 1524 in all domains.

1525

E ADDITIONAL EXPERIMENTAL RESULTS

1526 Here we provide more fine-grained statistics from the main experiments in the paper. Table 8 and 9
 1527 report the mean and max objectives, Vendi Score, and Coverage statistics of each algorithm in the
 1528 LP and LSI domains, respectively. Table 10 reports the QD Score and QVS from the IC experiments.
 1529 As noted in the paper, LP and IC results are averaged over 10 seeds and LSI results are averaged
 1530 over 5 seeds.

1531 We also provide hand-picked samples of the solutions found by SQuAD as well as the two best
 1532 baselines, CMA-MEGA and CMA-MAEGA, in both LSI tasks (Figure 6 and Figure 7) and the IC
 1533 domain (Figure 8). Lastly, Figure 9 compares the solutions found by SQuAD and CMA-M(A)EGA
 1534 in the LSI domain when they are put in a traditional CVT archive. Since this domain has a 2-d
 1535 behavior space, we can provide CVT archive visualizations for it.

1536 Table 8: Additional statistics from LP experiments.

| 1537 Algorithm | 1538 Mean Objective | 1539 Max Objective | 1540 Vendi Score | 1541 Coverage |
|-----------------------|----------------------------|---------------------------|-------------------------|----------------------|
| <i>easy (d = 4)</i> | | | | |
| SQUAD | 68.36 ± 0.02 | 89.28 ± 0.15 | 6.55 ± 0.01 | 86.4 ± 0.3 |
| CMA-MAEGA | 66.02 ± 0.28 | 91.00 ± 0.43 | 6.93 ± 0.05 | 98.7 ± 0.2 |
| CMA-MEGA | 66.40 ± 0.26 | 94.54 ± 0.38 | 7.61 ± 0.10 | 99.5 ± 0.2 |
| DNS | 68.07 ± 0.06 | 78.06 ± 0.04 | 1.63 ± 0.00 | 8.1 ± 0.2 |
| DNS-G | 78.23 ± 0.12 | 92.51 ± 0.09 | 1.35 ± 0.01 | 4.0 ± 0.1 |
| Sep-CMA-MAE | 69.81 ± 0.28 | 78.71 ± 0.29 | 1.25 ± 0.01 | 1.8 ± 0.0 |
| GA-ME | 69.76 ± 0.95 | 79.42 ± 0.21 | 1.07 ± 0.01 | 0.9 ± 0.0 |
| <i>medium (d = 8)</i> | | | | |
| SQUAD | 69.41 ± 0.02 | 87.70 ± 0.36 | 9.17 ± 0.02 | 93.1 ± 0.2 |
| CMA-MAEGA | 62.12 ± 0.20 | 84.41 ± 0.33 | 9.27 ± 0.05 | 100.0 ± 0.0 |
| CMA-MEGA | 62.13 ± 0.67 | 86.76 ± 0.70 | 7.58 ± 0.19 | 99.9 ± 0.1 |
| DNS | 66.87 ± 0.08 | 77.61 ± 0.07 | 1.67 ± 0.00 | 13.4 ± 0.2 |
| DNS-G | 75.96 ± 0.07 | 91.41 ± 0.22 | 1.43 ± 0.00 | 7.5 ± 0.2 |
| Sep-CMA-MAE | 66.49 ± 1.42 | 77.04 ± 0.13 | 1.25 ± 0.02 | 1.1 ± 0.15 |
| GA-ME | 69.48 ± 1.08 | 78.99 ± 0.16 | 1.07 ± 0.01 | 0.6 ± 0.0 |
| <i>hard (d = 16)</i> | | | | |
| SQUAD | 72.86 ± 0.01 | 83.92 ± 0.21 | 6.61 ± 0.01 | 91.1 ± 0.2 |
| CMA-MAEGA | 64.76 ± 2.04 | 81.27 ± 0.66 | 4.59 ± 0.73 | 71.8 ± 13.3 |
| CMA-MEGA | 58.11 ± 0.39 | 76.19 ± 0.38 | 3.73 ± 0.08 | 99.8 ± 0.1 |
| DNS | 66.19 ± 0.04 | 77.13 ± 0.07 | 1.69 ± 0.00 | 60.5 ± 0.8 |
| DNS-G | 74.29 ± 0.09 | 90.54 ± 0.15 | 1.45 ± 0.00 | 56.2 ± 0.7 |
| Sep-CMA-MAE | 65.04 ± 0.84 | 78.87 ± 0.11 | 1.33 ± 0.01 | 4.7 ± 0.6 |
| GA-ME | 78.83 ± 0.66 | 89.76 ± 0.17 | 1.08 ± 0.00 | 3.8 ± 0.5 |

1566
1567
1568 Table 9: Additional statistics from LSI experiments.
1569
1570
1571
1572
1573
1574
1575
1576
1577

| Algorithm | Mean Objective | Max Objective | Vendi Score | Coverage |
|-------------------|----------------------|----------------------|-----------------|----------------|
| <i>LSI</i> | | | | |
| SQUAD | 79.56 ± 0.45 | 83.81 ± 0.09 | 2.22 ± 0.03 | 32.4 ± 0.5 |
| CMA-MAEGA | 77.18 ± 3.96 | 86.98 ± 0.45 | 1.57 ± 0.07 | 15.9 ± 2.0 |
| CMA-MEGA | 83.38 ± 0.89 | 87.46 ± 0.06 | 1.68 ± 0.01 | 19.7 ± 0.2 |
| DNS | -221.24 ± 28.01 | 84.10 ± 0.11 | 1.39 ± 0.00 | 10.2 ± 0.3 |
| DNS-G | -288.33 ± 26.12 | 85.22 ± 0.05 | 1.36 ± 0.00 | 9.3 ± 0.0 |
| Sep-CMA-MAE | -476.62 ± 241.08 | -139.05 ± 135.77 | 1.01 ± 0.01 | 0.4 ± 0.1 |
| GA-ME | -558.40 ± 68.50 | 83.72 ± 0.10 | 1.25 ± 0.01 | 6.8 ± 0.3 |
| <i>LSI (hard)</i> | | | | |
| SQUAD | 82.51 ± 0.01 | 84.26 ± 0.09 | 1.83 ± 0.00 | 6.0 ± 0.2 |
| CMA-MAEGA | 81.55 ± 1.25 | 87.05 ± 0.12 | 1.22 ± 0.02 | 0.9 ± 0.2 |
| CMA-MEGA | 84.24 ± 0.52 | 85.98 ± 0.2 | 1.10 ± 0.02 | 0.6 ± 0.1 |
| DNS | -222.68 ± 12.24 | 84.02 ± 0.04 | 1.38 ± 0.00 | 10.2 ± 0.2 |
| DNS-G | -214.70 ± 35.08 | 85.17 ± 0.03 | 1.35 ± 0.01 | 9.1 ± 0.2 |
| Sep-CMA-MAE | -37.6 ± 94.16 | 16.74 ± 42.55 | 1.00 ± 0.00 | 0.2 ± 0.0 |
| GA-ME | -168.09 ± 217.38 | 83.46 ± 0.14 | 1.04 ± 0.01 | 0.2 ± 0.0 |

1578
1579
1580
1581
1582
1583
1584
1585
1586
1587
1588
1589
1590
1591
1592
1593
1594
1595
1596
1597
1598
1599
1600
1601
1602
1603
1604
1605
1606
1607
1608
1609
1610
1611
1612
1613
1614
1615
1616
1617
1618
1619
Table 10: Additional statistics from IC experiments.

| Algorithm | QD Score | QVS |
|-------------|--------------------|-------------------|
| SQUAD | 5086.2 ± 54.7 | 457.35 ± 0.23 |
| CMA-MAEGA | 4605.8 ± 40.5 | 294.07 ± 1.96 |
| CMA-MEGA | 3565.7 ± 386.2 | 246.89 ± 17.7 |
| DNS | 1128.4 ± 15.7 | 115.17 ± 0.65 |
| DNS-G | 1148.0 ± 24.2 | 124.72 ± 0.33 |
| Sep-CMA-MAE | 348.9 ± 17.6 | 94.735 ± 0.8 |
| GA-ME | 140.9 ± 23.2 | 83.43 ± 2.97 |

F STATEMENT ON GENERATIVE AI USAGE

Generative AI tools were used as an aid to improve clarity and style in the writing of this paper.

G RUNTIME ANALYSIS

Table 11 summarizes the wall clock runtimes for SQUAD and all baselines on the three domains we consider. The most influential factor in SQUAD’s runtime is the cost of gradient computation. In the Rastrigin domains this cost is relatively small. Therefore, even in the hard setting where the behavior space has dimension 16, SQUAD completes all 1000 iterations in under one minute. In these domains the computational structure is simple and backpropagation is inexpensive, which leads to very fast overall runtime.

In contrast, the IC and LSI domains require gradients that must be backpropagated through significantly more complex computational pipelines. In IC, each gradient step involves differentiation through a differentiable renderer. In LSI, gradients pass through both StyleGAN and CLIP, which are large networks and therefore incur substantial computational overhead. As a result, the wall clock times for SQUAD in these two domains are noticeably higher.

It is important to emphasize that these higher runtimes do not indicate inefficiency of SQUAD. In fact, SQUAD converges very quickly to high-quality solutions. Figure 10 shows the training curves of SQUAD together with the final performance of all baselines in terms of QD Score and QVS in the IC domain. SQUAD surpasses all baselines in both metrics in fewer than 200 iterations. Nevertheless, we ran SQUAD for 1000 iterations primarily to ensure an equal evaluation budget

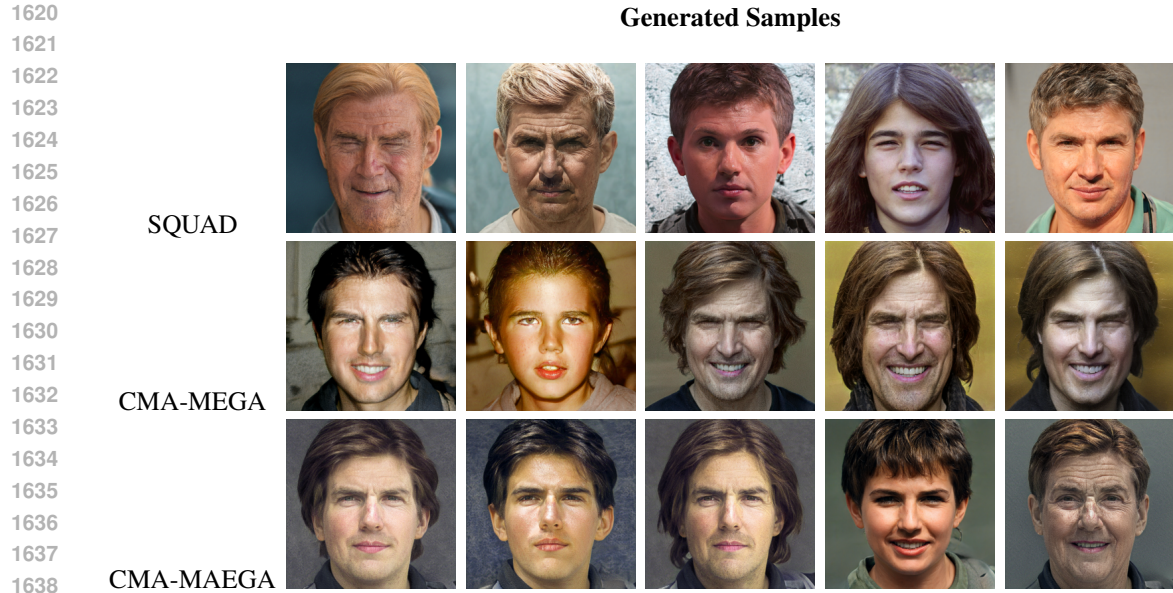


Figure 6: Qualitative comparison of SQUAD against two baselines in LSI. Each row corresponds to one algorithm, with five representative samples handpicked from the populations.

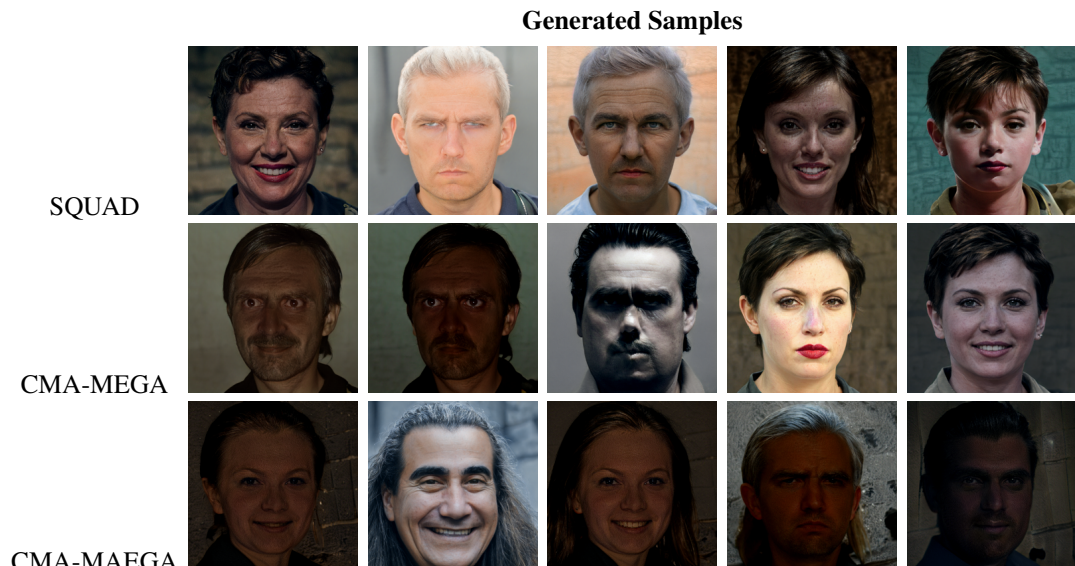


Figure 7: Qualitative comparison of SQUAD against two baselines in LSI (hard). Each row corresponds to one algorithm, with five representative samples handpicked from the populations.

across algorithms. In practice, one can use SQUAD with a far smaller number of iterations and still obtain superior results, which directly reduces the wall clock time below the values reported in the table above.

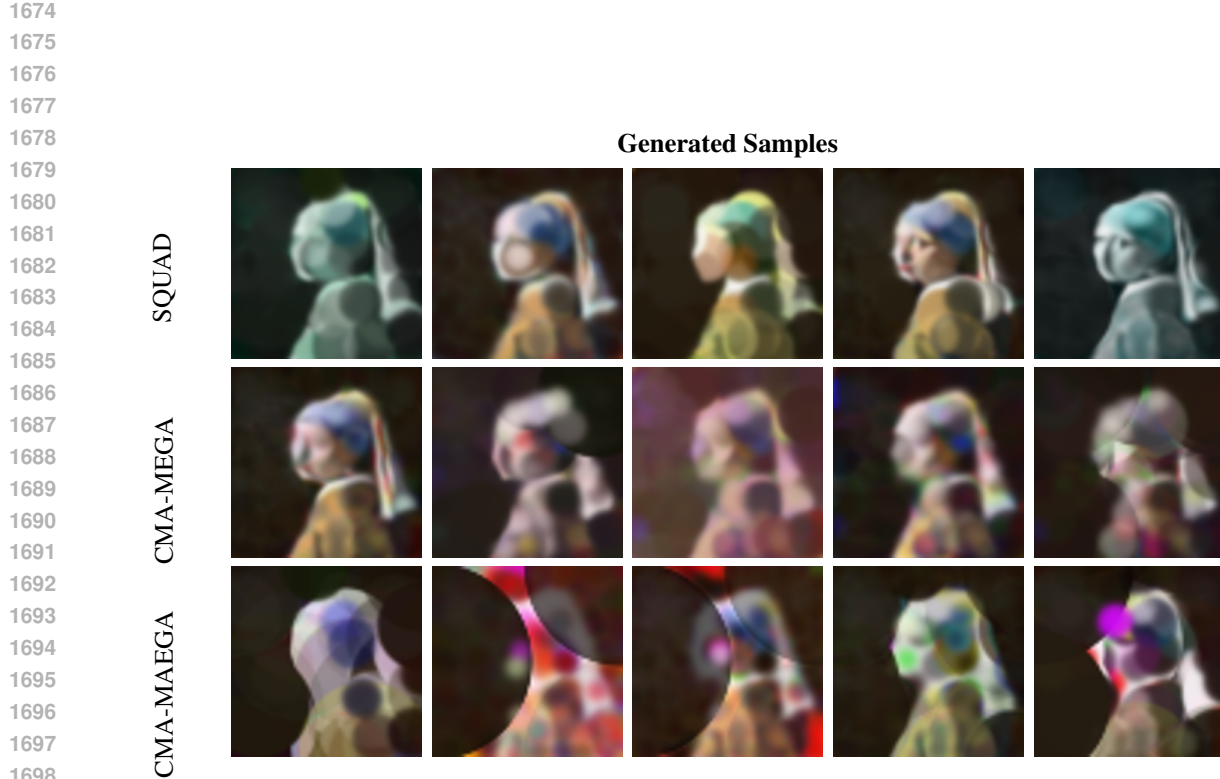


Figure 8: Qualitative comparison of SQUAD against two baselines in IC. Each row corresponds to one algorithm, with five representative samples handpicked from the populations.

Table 11: Wall clock runtime (in minutes) of SQUAD and all baselines across the three domains. For Rastrigin we report runtimes for the easy, medium, and hard settings. For LSI we report the base and hard settings.

| Method | Rastrigin | | | IC | | LSI | |
|-------------|-----------|--------|------|------|------|------|--|
| | Easy | Medium | Hard | Base | Hard | | |
| SQUAD | <1 | <1 | <1 | 190 | 732 | 1316 | |
| GA-ME | 1 | 3 | 17 | 66 | 403 | 707 | |
| CMA-MAEGA | 45 | 78 | 66 | 8 | 222 | 339 | |
| CMA-MEGA | 64 | 66 | 106 | 8 | 233 | 337 | |
| DNS | 5 | 8 | 10 | 6 | 15 | 25 | |
| DNS-G | 3 | 4 | 5 | 50 | 207 | 355 | |
| Sep-CMA-MAE | 1 | 3 | 33 | 5 | 8 | 10 | |

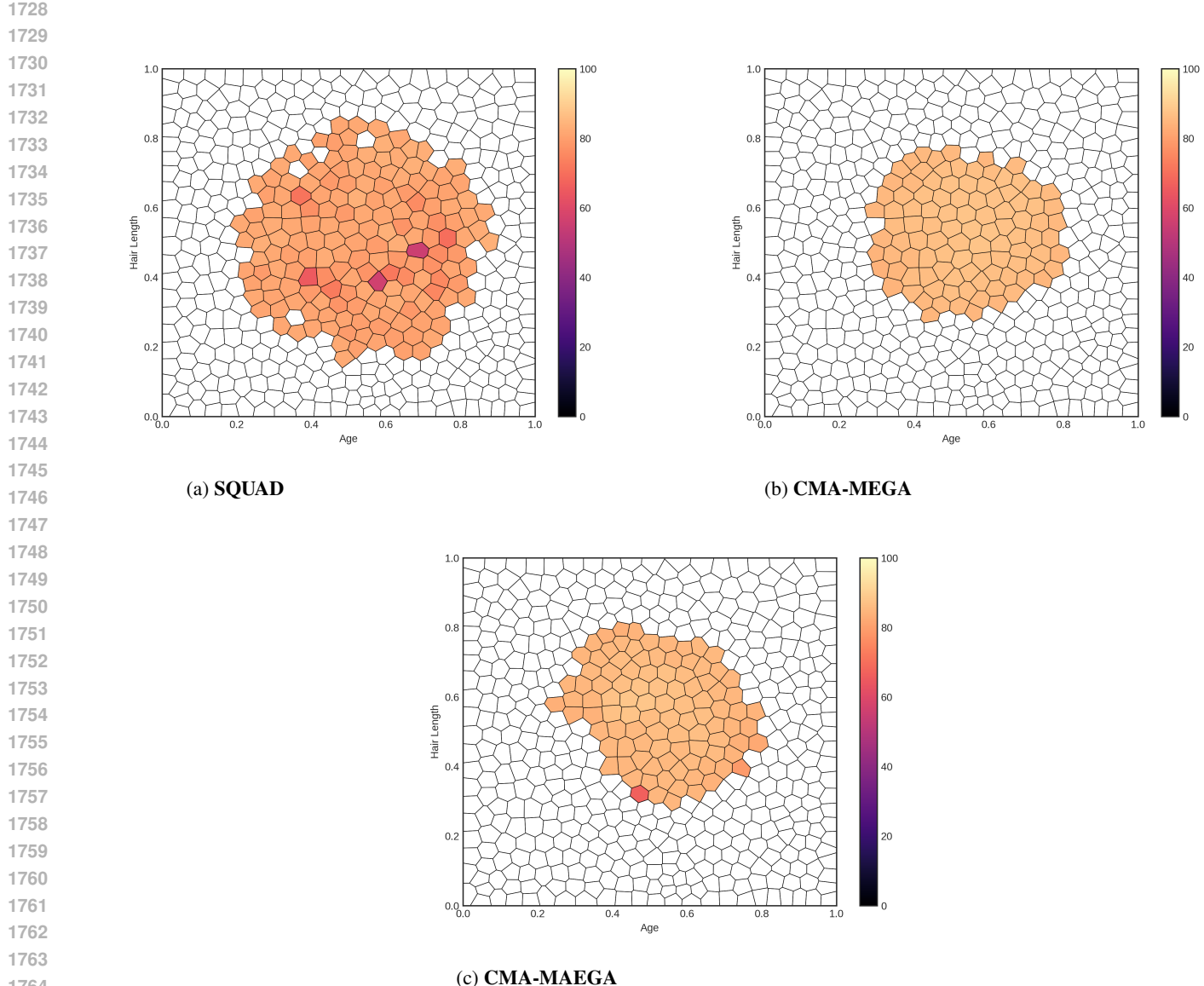


Figure 9: Final CVT archives of SQUAD, CMA-MEGA, and CMA-MAEGA in the LSI domain.

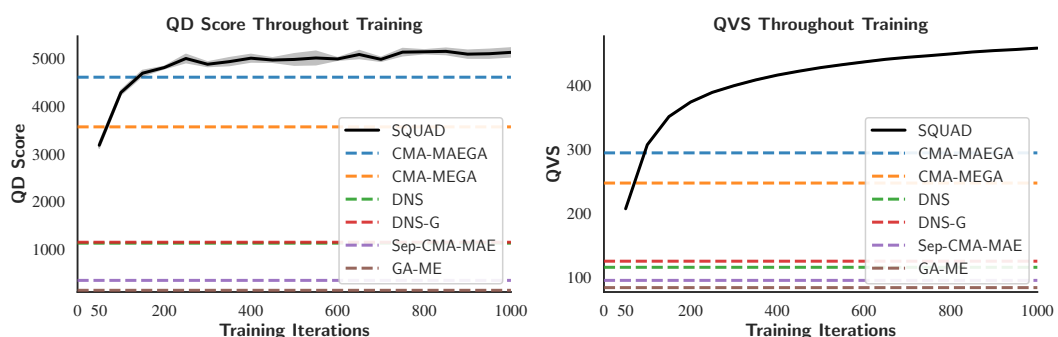


Figure 10: Training curves for SQUAD compared with the final QD Score and QVS values of all baselines in the IC domain. SQUAD exceeds all baselines on both metrics in fewer than 200 iterations.